Phosphorylation of PSD-95 at Serine 73 in dCA1 is required for extinction of contextual fear

Authors

Magdalena Ziółkowska[&,1], Malgorzata Borczyk[&,1,2], Anna Cały[1], Maria Nalberczak-Skóra[1], Agata Nowacka[1], Małgorzata Alicja Śliwińska[1,3], Kacper Łukasiewicz[1], Edyta Skonieczna[1], Kamil F. Tomaszewski[1], Tomasz Wójtowicz[4], Jakub Włodarczyk[4], Tytus Bernaś[3,5], Ahmad Salamian[1] and Kasia Radwanska[1*].

Affiliations

[1]Laboratory of Molecular Basis of Behavior, the Nencki Institute of Experimental Biology of Polish Academy of Sciences.

[2]Department Molecular Neuropharmacology, Maj Institute of Pharmacology of Polish Academy of Sciences, Warsaw, Poland.

[3]Laboratory of Imaging Tissue Structure and Function, The Nencki Institute of Experimental Biology of Polish Academy of Sciences, Warsaw, Poland.

[4]Laboratory of Cell Biophysics, the Nencki Institute of Experimental Biology of Polish Academy of Sciences.

[5]Department of Anatomy and Neurology, VCU School of Medicine, 1101 East Marshall Street, Richmond, Virginia 23298.

[&]equal contribution.

*__Corresponding author__: Kasia Radwanska, Ph.D., Laboratory of Molecular Basis of Behavior, Nencki Institute of Experimental Biology of Polish Academy of Sciences, 3 Pasteur St., Warsaw 02-093, Poland; e-mail: k.radwanska@nencki.edu.pl; tel: +48501736942.

Key words: PSD-95, fear extinction, dorsal CA1, synaptic plasticity, hippocampus, αCaMKII

Running title: Synaptic plasticity is required for fear extinction.

Number of pages: 35

Number of figures, tables, multimedia and 3D models (separately)

Figures (6), tables (0), multimedia and 3D models (0), supplementary figures (3)

Number of words for Abstract, Introduction, and Discussion (separately)

Abstract (113), Introduction (682), Discussion (1374)

ABSTRACT

The updating of contextual memories is essential for survival in a changing environment. Accumulating data indicate that the dorsal CA1 area (dCA1) contributes to this process. However, the cellular and molecular mechanisms of contextual fear memory updating remain poorly understood. Postsynaptic density protein 95 (PSD-95) regulates the structure and function of glutamatergic synapses. Here, using dCA1-targeted genetic manipulations *in vivo*, combined with *ex vivo* 3D electron microscopy and electrophysiology, we identify a novel, synaptic mechanism that is induced during attenuation of contextual fear memories and involves phosphorylation of PSD-95 at Serine 73 in dCA1. Our data provide the proof that PSD-95-dependent synaptic plasticity in dCA1 is required for updating of contextual fear memory.

INTRODUCTION

The ability to form, store, and update memories is essential for animal survival. In mammals, the formation, recall and updating of memories involve the hippocampus (Frankland and Bontempi, 2005; Neves et al., 2008; Baldi and Bucherelli, 2015). In particular, formation of memories strengthens the Schaffer collateral-to-dorsal CA1 area (dCA1) synapses through N-methyl-D-aspartate receptor (NMDAR)-dependent forms of synaptic plasticity (Bliss and Collingridge, 1993; Morris et al., 2003; Abraham et al., 2019) linked with growth and addition of new dendritic spines (harbouring glutamatergic synapses) (Restivo et al., 2009; Radwanska et al., 2011; Mahmmoud et al., 2015; Aziz et al., 2019). Although some studies also found long-term depression of synaptic transmission during hippocampal-dependent tasks (Kemp and Manahan-Vaughan, 2007; Goh and Manahan-Vaughan, 2013). Similarly, updating and extinction of memories induces functional, structural, and molecular alterations of dCA1 synapses (Garín-Aguilar et al., 2012; Stansley et al., 2018; Schuette et al., 2020). Accordingly, NMDAR-dependent plasticity of dCA1 synapses is commonly believed to be a primary cellular learning mechanism. Surprisingly, the role of dCA1 synaptic plasticity in memory formation has been recently questioned. Local genetic manipulations that impair synaptic function and plasticity specifically in dCA1 affect spatial choice and incorporation of salience information into cognitive representations, rather than formation of cognitive maps and memory engrams (Bannerman et al., 2012, 2014; Hirsch et al., 2015; Cały et al., 2021; Kaganovsky et al., 2022). On the other hand, the

role of dCA1 synaptic plasticity in the updating and extinction of existing hippocampus-dependent memories has not been tested yet. Understanding the molecular and cellular mechanisms that underlie fear extinction memory is crucial to develop new therapeutic approaches to alleviate persistent and unmalleable fear memories.

PSD-95 is the major scaffolding protein of glutamatergic synapses (Cheng et al., 2006). It directly interacts with NMDARs and with AMPARs through an auxiliary protein, stargazin (Kornau et al., 1995; Schnell et al., 2002). Interaction of PSD-95 with stargazin regulates the synaptic content of AMPARs (Chetkovich et al., 2002; Schnell et al., 2002; Bats et al., 2007). Accordingly, PSD-95 affects stability and maturation as well as functional and structural plasticity of glutamatergic synapses (Migaud et al., 1998; Béïque and Andrade, 2003; Stein et al., 2003; Ehrlich and Malinow, 2004; Ehrlich et al., 2007; Nikonenko et al., 2008; Steiner et al., 2008; Sturgill et al., 2009; Chen et al., 2011; Taft and Turrigiano, 2014). Synaptic localisation of PSD-95 is controlled by a range of posttranslational modifications with opposing effects on its synaptic retention as well as synaptic function and plasticity (Vallejo et al., 2017). Here, in order to test the role of dCA1 excitatory synapses in extinction of fear memories, we focused on phosphorylation of PSD-95 at Serine 73 (S73). Phosphorylation of PSD-95(S73) enables PSD-95 dissociation from the complex with GluN2B, and its trafficking to terminate synaptic growth after stimulation of NMDA receptors, and is necessary for PSD-95 protein downregulation during NMDAR-dependent long-term depression of synaptic transmission (LTD) (Steiner et al., 2008; Nowacka et al., 2020). PSD-95(S73) is phosphorylated by the calcium and calmodulin-dependent kinase II (CaMKII) (Gardoni et al., 2006; Steiner et al., 2008). Importantly, both authophosphorylation-deficient αCaMKII mutant mice (αCaMKII-T286A) (Giese et al., 1998) and the loss-of-function PSD-95 mutants lacking the guanylate kinase domain of PSD-95 (Migaud et al., 1998) show impaired extinction of contextual fear (Radwanska et al., 2011; Fitzgerald et al., 2015), suggesting that αCaMKII and PSD-95 interact to regulate contextual fear extinction.

The present study tests the role of PSD-95(S73) phosphorylation in the dorsal hippocampus in fear memory extinction by integrated analyses of PSD-95 protein expression and phosphorylation, dCA1-targeted expression of phosphorylation-deficient PSD-95 protein (with serine 73 mutated to alanine, S73A) as well as examination of dendritic spines morphology with nanoscale resolution enabled by electron microscopy. We show that phosphorylation of PSD-95(S73) is necessary for contextual fear extinction-induced PSD-95 protein regulation and remodelling of glutamatergic

synapses. Moreover, it is not necessary for fear memory formation but required for fear extinction even after extensive fear extinction training. Overall, our data show for the first time that the dCA1 PSD-95(S73) phosphorylation is required for extinction of the contextual fear memory.

RESULTS

The contextual fear extinction affects PSD-95 protein levels and morphology of dendritic spines in dCA1.

To investigate the role of dCA1 excitatory synapses in contextual fear memory extinction, we trained Thy1-GFP(M) mice (that allow for visualisation of dendritic spines) (Feng et al., 2000) in contextual fear conditioning (CFC). The animals showed low freezing levels in the novel context before delivery of 5 electric shocks (US), after which the freezing levels increased during the rest of the training session (**Figure** 1A). Twenty-four hours later, one group of mice was sacrificed (5US) (mice were randomly assigned to the experimental groups), and the second group was re-exposed to the training context for 30 minutes without presentation of US for extinction of contextual fear (Ext). Freezing levels were high at the beginning of the session and decreased within the session indicating formation of fear extinction memory ($t = 3.720$, $df = 6$, $P < 0.001$). Mice were sacrificed immediately after the fear extinction session. Twenty-four hours later, the third group of mice was re-exposed to the training context (without US) to test consolidation of fear extinction memory (test). Freezing levels were lower during the test as compared to the beginning of the extinction, indicating that our protocol resulted in efficient formation of long-term contextual fear extinction memory ($P = 0.026$). The mouse brains were sliced, the brain sections immunostained to detect PSD-95 protein using specific antibodies and imaged with a confocal microscope. The scans were analysed to asses PSD-95 protein levels [linear density of PSD-95-positive puncta (PSD-95^+) per 1 µm of a dendrite and mean grey value of PSD-95^+ per dendritic spine] and dendritic spines linear density and area [enabled by Thy1-GFP(M) transgene] (**Figure** 1B-C). As dendritic spines change in dCA1 after CFC in a dendrite-specific manner (Restivo et al., 2009), the expression of PSD-95 protein, and its colocalization with dendritic protrusions, were analysed in three domains of dCA1: stratum oriens (stOri), stratum radiatum (stRad) and stratum lacunosum-moleculare (stLM) (**Figure** 1D-F).

The analysis of the confocal scans revealed that there were less PSD-95$^+$ puncta after fear extinction, as compared to the 5US group in stOri, but not in other dCA1 strata (**Figure** 1G). There was also a significant effect of the training on PSD-95 protein levels per dendritic spine. In the stOri and stLM, PSD-95 levels per dendritic spine increased after extinction, as compared to the 5US group (**Figure** 1H). No difference in PSD-95 levels per dendritic spine was observed between the groups in stRad. Interestingly, when total PSD-95 levels were analysed (as mean grey value of microphotographs) we found no differences between the experimental groups in three strata of dCA1 (**Figure** 1I), indicating bidirectional PSD-95 changes (elimination of PSD-95$^+$ puncta and increased intensity of the remaining puncta).

Next, we checked whether the changes in PSD-95 protein levels were associated with dendritic spine remodelling. In stOri, dendritic spine density decreased after extinction as compared to the 5US mice (**Figure** 1J). No changes in dendritic spine density were observed in the stRad and stLM. Moreover, the median dendritic spine area was increased in stOri after extinction, compared to the 5US group, resembling the changes of PSD-95 protein levels. No changes in the median dendritic spine area were observed in the stRad and stLM (**Figure** 1K). In a separate experiment we found that these dendritic spine changes were transient, as they were not observed 60 minutes after contextual fear extinction session, and they were specific for fear extinction, as we did not find such changes in the animals exposed to a neutral novel context (not associated with US) as compared to 5US group (**Supplementary Figure** 1).

Overall, our data indicate that contextual fear extinction involves transient remodelling of the stOri neuronal circuit characterised by decreased density of dendritic spines with PSD-95 and upregulation of PSD-95 protein levels in the remaining dendritic spines. No significant synaptic changes were found in stRad, and only changes of PSD-95 in stLM.

Synaptic changes in dCA1 during contextual fear extinction are homeostatic.

Since we observed significant changes of dendritic spines and PSD-95 protein levels in dCA1 after fear extinction, in the following experiment we tested whether contextual fear extinction affected synaptic strength in dCA1 strata. To this end, field excitatory postsynaptic potentials (fEPSPs) were measured in acute hippocampal slices when the Shaffer collateral was stimulated by monotonically

increasing stimuli (**Supplementary Figure** 2). The input-output curves showed no significant differences in the amplitude of fEPSP and fibre volley in stOri, stRad and stLM between the mice sacrificed immediately before or after fear extinction session (**Supplementary Figure** 2), indicating no global changes in synaptic strength. Thus our data indicate that extinction-induced remodelling of dendritic spines was homeostatic.

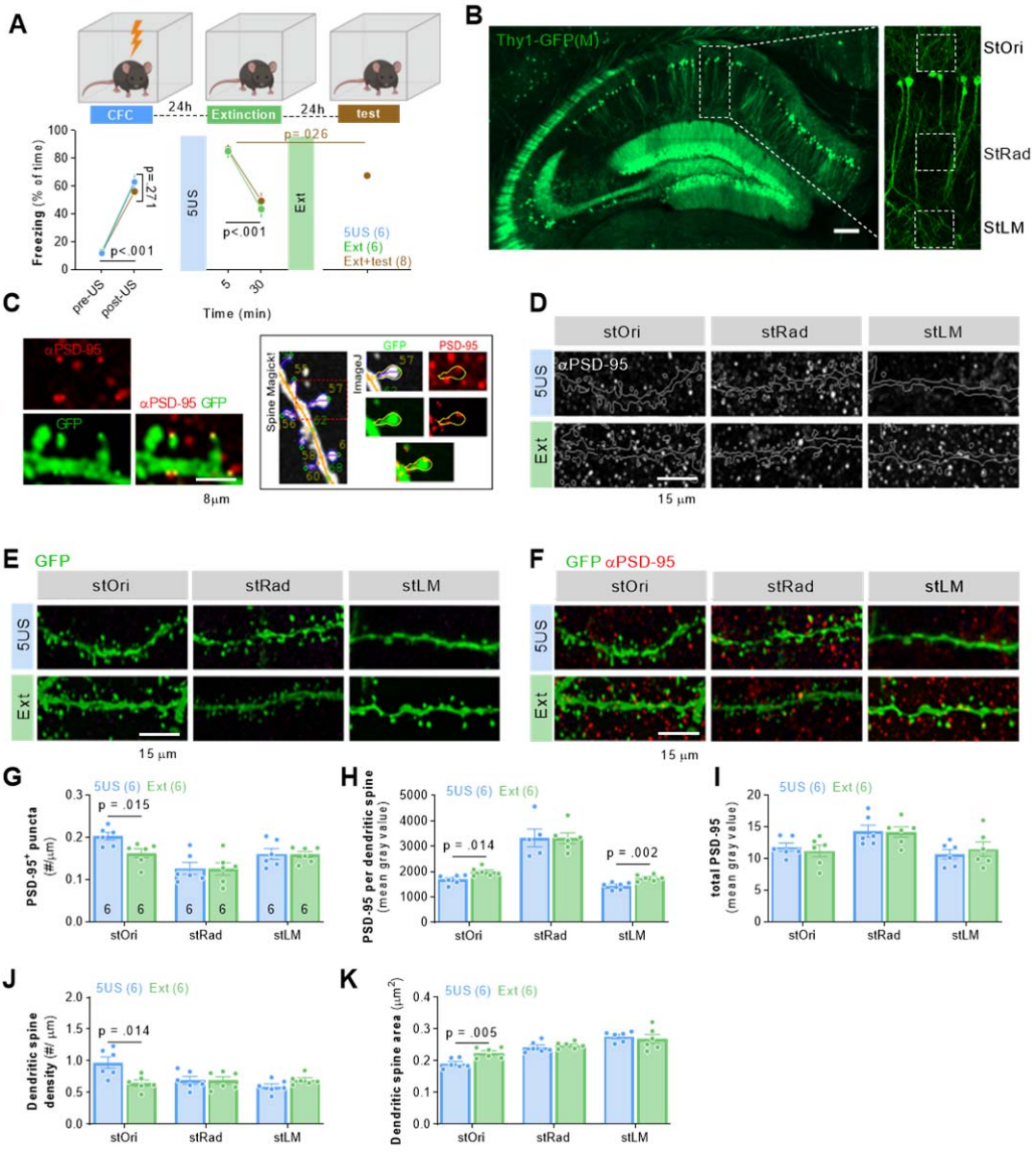

Figure 1. Extinction of contextual fear memory regulates PSD-95 protein levels and remodelling of dendritic spines in dCA1. (A) Experimental timeline and freezing levels during training. Mice underwent CFC and were sacrificed 24 hours later (5US, n = 6) or after re-exposure to the training context without electric shocks (Ext, n = 6) (two-way repeated-measures ANOVA, effect of training:

F(1, 10) = 77.86, P < 0.0001). **(B-C)** Dendritic spines and PSD-95 expression were analysed in three domains of the dendritic tree of dCA1 pyramidal neurons (stOri, stRad and stLM) in Thy1-GFP(M) male mice. **(B)** Microphotography of dCA1 and dendritic tree domains. **(C)** High magnification of confocal scans showing colocalization of PSD-95 immunostaining and dendritic spines, and the analysis in SpineMagick! and ImageJ. **(D-F)** Representative confocal images (maximum projections of z-stacks composed of 20 scans) of PSD-95 immunostaining, GFP and their colocalization are shown for three domains of dCA1. Scale bar, 15 µm. **(G-I)** Summary of data showing density of PSD-95$^+$ puncta (two-way repeated-measures ANOVA with Tukey's multiple comparisons test (marked on the graphs), effect of training: F(2, 13) = 1.30, P = 0.305), PSD-95 expression per dendritic spine (effect of training: F(2, 15) = 5.653, P = 0.015) and total PSD-95 expression (effect of training: F(2, 14) = 1.126, P = 0.3521). **(J-K)** Summary of data showing dendritic spine density (effect of training: F(2, 44) = 2.851, P = 0.069; a region effect: F(1.983, 43.63) = 6.293, P = 0.004; training × region interaction: F(4, 44) = 5.389, P = 0.001) and average dendritic spine area (two-way repeated-measures ANOVA with Tukey's multiple comparisons test; effect of training: F(2, 42) = 1.630, P = 0.208; a region effect: F(2, 42) = 46.49, P < 0.001; training × region interaction: F(4, 42) = 2.121, P = 0.095). The analyses were conducted in stOri (mouse/dendrite/spine: 5US = 6/25/650; Ext = 6/37/925). For G-I, each dot represents one mouse. For G-J, M means ± SEM are shown. For K, medians ± IQR are shown.

Contextual fear extinction induces phosphorylation of PSD-95(S73) in dCA1

Phosphorylation of PSD-95(S73) has been associated with various forms of synaptic plasticity (Gardoni et al., 2006; Nowacka et al., 2020). To test whether contextual fear extinction induces phosphorylation of PSD-95(S73) in dCA1, we generated an antibody directed against this phosphorylation site (**Figure** 2A) (Gardoni et al., 2006). Mice underwent CFC and were sacrificed 24 hours later (5US), or after 15 or 30 minutes of the contextual fear extinction session (Ext15' or Ext30') (**Figure** 2B). The levels of PSD-95, phosphorylated PSD-95(S73) [phospho-PSD-95(S73)] and their colocalization were tested on the brain sections (**Figure** 2C). Total PSD-95, phospho-PSD-95(S73) and their colocalization levels were higher in the Ext15', but not Ext30', group as compared to the 5US animals (**Figure** D-F). Thus our data indicate that the alteration of PSD-95 protein levels during contextual fear extinction was accompanied by transiently increased phosphorylation of PSD-95(S73).

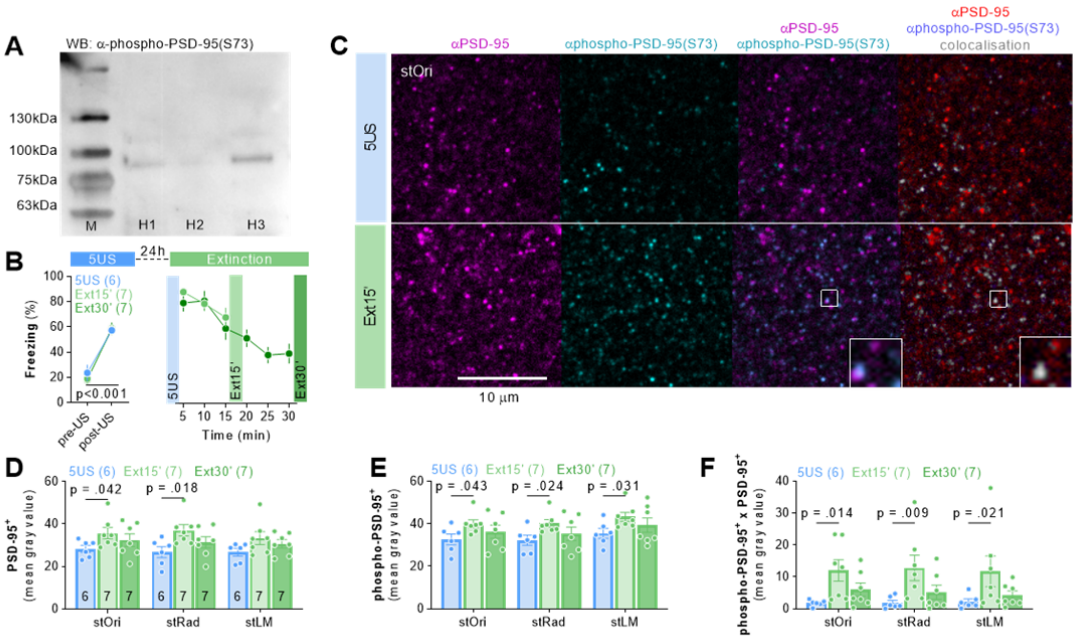

Figure 2. Contextual fear extinction induces transient phosphorylation of PSD-95(S73) in dCA1.

(A) Western blot stained with phospho-PSD-95(S73)-specific antibody detects in the hippocampus homogenates (H1-3) proteins with approx. 95 kDA molecular weight. M, molecular weight marker. **(B)** Experimental timeline and freezing levels during training. Mice underwent CFC and were sacrificed 24 hours later (5US, n = 6) or after 15 or 30 minutes of a fear extinction session (Ext15', n = 7; Ext30', n = 7). **(C)** Representative confocal scans of the brain slices (stOri) immunostained with antibodies specific for PSD-95, phosphorylated PSD-95(S73) and their colocalization. **(D-F)** Quantification of the PSD-95 (two-way ANOVA, effect of training: $F(2, 17) = 2.69$, $P = 0.097$; effect of stratum: $F(1,96, 33,3) = 3.83$, $P = 0.033$), phospho-PSD-95(S73) (two-way ANOVA, effect of training: $F(2, 17) = 2.20$, $P = 0.141$; effect of stratum: $F(1,24, 21,0) = 24.9$, $P < 0.001$) and their colocalization levels (two-way ANOVA, effect of training: $F(2, 17) = 4.08$, $P = 0.036$; effect of stratum: $F(2, 34) = 0.169$, $P = 0.845$). Each dot represents one mouse. Means ± SEM are shown.

PSD-95(S73) phosphorylation regulates PSD-95 protein levels during contextual fear extinction.

To test whether phosphorylation of PSD-95(S73) regulates PSD-95 protein levels in dCA1 during fear extinction we used dCA1-targeted expression of phosphorylation-deficient PSD-95 with S73 mutated to alanine (S73A). We designed and produced adeno-associated viral vectors (AAV1/2) encoding wild-type PSD-95 protein under *Camk2a* promoter fused with mCherry (AAV1/2:CaMKII_PSD-95(WT):mCherry) (WT) or PSD-95(S73A) fused with mCherry (AAV1/2:CaMKII_PSD-95(S73A):mCherry) (S73A) (Nowacka et al., 2020) (**Supplementary Figure** 3). Mice underwent CFC (**Figure** 3A). The animals in all experimental groups showed increased freezing levels at the end of the training. Half of the mice were sacrificed 24 hours after CFC (5US). The remaining half were sacrificed after the 30-minut contextual fear extinction session (Ext). All animals

showed high freezing levels at the beginning of the session, which decreased during the session. No effect of the virus was found (**Figure** 3A).

For each animal, half of the brain was chosen at random for confocal analysis of the PSD-95 protein levels, and the other half was processed for Serial Block-face Scanning Electron Microscopy (SBEM) (**Figure** 3B). The AAVs penetrance did not differ between the experimental groups (5US vs Ext) and reached over 80% of the cells in the analysed sections of dCA1 (**Figure** 3C). Correlative light and electron microscopy confirmed that the exogenous PSD-95 co-localised with postsynaptic densities (PSDs) representing a postsynaptic part of excitatory synapses, and only weak signal was present in dendrites (**Figure** 3D). We did not observe significant differences in total PSD-95 protein levels between the WT and S73A mice sacrificed before the fear extinction session. The total PSD-95 protein levels were not changed after fear extinction in the WT group, as compared to the WT mice sacrificed before the fear extinction session. However, PSD-95 levels were upregulated in all strata after the extinction session in the S73A mice, as compared to the WT Ext animals and the S73A 5US group (**Figure** 3F). As no significant differences in the mean PSD-95^{+} area were observed between the WT Ext and S73A Ext mice (**Figure** 3G), the differences in total PSD-95 levels likely resulted from higher density of PSD-95^{+} puncta in the S73A Ext group as compared to the S73A 5US and WT Ext animals (**Figure** 3F). Hence, exogenous PSD-95(S73A) protein impaired regulation of PSD-95^{+} density, indicating that phosphorylation of PSD-95(S73) controls PSD-95 levels during fear extinction.

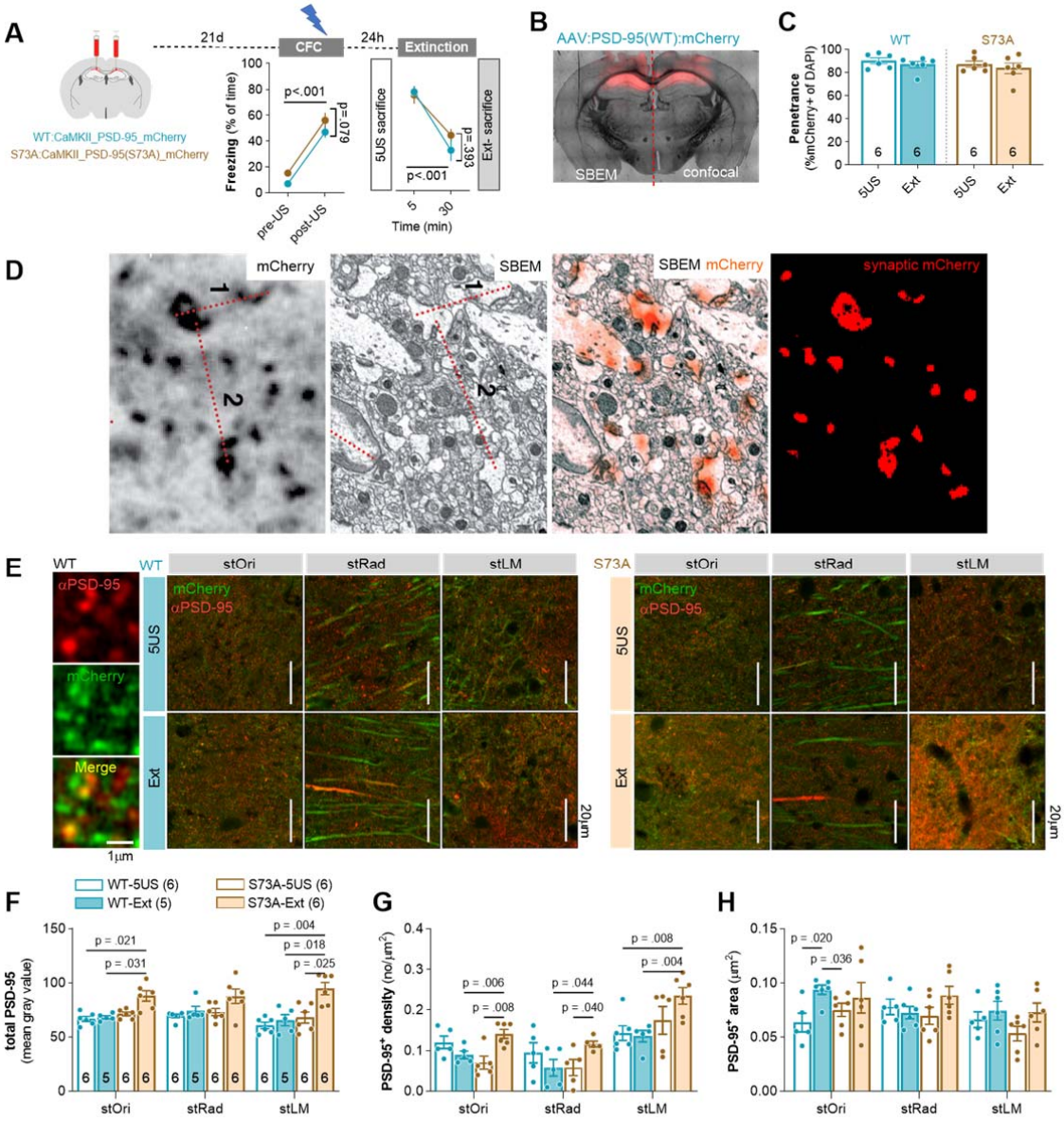

Figure 3. PSD-95(S73) is phosphorylated during fear extinction and this process is required for regulation of PSD-95 protein levels. (A) Experimental timeline and freezing during training. C57BL/6J male mice were stereotactically injected in the dCA1 with AAV1/2 encoding PSD-95(WT) (WT, n = 12) or PSD-95(S73A) (S73A, n = 12). Twenty one days later they underwent CFC (two-way repeated-measures ANOVA, effect of training: $F(1, 30) = 269.4$, $P < 0.001$, effect of virus: $F(2, 30) = 2.815$, $P = 0.076$) and were sacrificed 1 day after training (5US) or they were re-exposed to the training context without footshock and sacrificed (Ext) (two-way repeated-measures ANOVA, effect of training: $F(1, 15) = 65.68$, $P < 0.001$; effect of virus: $F(2, 15) = 0.993$, $P = 0.393$). **(B)** Microphotography of a brain with dCA1 PSD-95(WT):mCherry expression with illustration of the brain processing scheme**. (C)** Summary of data showing the viruses penetrance in dCA1 (sections used for confocal and SBEM analysis) (mice: 5US/Ext, WT = 6/5; S73A = 6/6). **(D)** Correlative confocal-electron microscopy analysis showing that exogenous PSD-95(WT) co-localises with PSDs. Single confocal scan of an exogenous PSD-95(WT) in dCA1, SBEM scan of the same area, superposition of confocal (orange) and SBEM images based on measured distances between large synapses (1 & 2), and thresholded synaptic PSD-95(WT) signal. Measurements: (confocal image) 1: 3.12 µm, 2: 4.97

μm; (SBEM image) 1: 2.98 μm, 2: 4.97 μm. **(E-H)** Analysis of PSD-95 expression after fear extinction training. **(E)** Representative confocal scans of the PSD-95 immunostaining. Means ± SEM are shown.

Phosphorylation of PSD-95(S73) regulates stOri synapses during fear extinction.

To test whether phosphorylation of PSD-95(S73) regulates structural plasticity of excitatory synapses during contextual fear extinction we used SBEM. We reconstructed dendritic spines and PSDs in the stOri and determined dendritic spine density and volume as well as PSDs surface area [as a proxy of synaptic strength (Nusser et al., 1998; Noguchi et al., 2005; Katz et al., 2009)] and volume [as a proxy of the accumulated synaptic proteins (Borczyk et al., 2019)] (**Figure** 4A-D). In total, we reconstructed 159 spines from the brains of the WT mice sacrificed 24 hours after CFC (5US) (n=3), and 178 spines from the mice sacrificed after fear extinction (Ext) (n=3). For mice expressing S73A, 183 spines were reconstructed in the 5US group (n=3) and 160 Ext (n=3). Figure 4D shows reconstructions of dendritic spines from representative SBEM brick scans for each experimental group.

Dendritic spine density was lower in the WT Ext group, as compared to the WT 5US mice (**Figure** 4E). Furthermore, the median values of dendritic spine volume, PSD surface area and PSD volume were higher after the extinction training in the WT group, as compared to the WT 5US mice. These changes were also indicated as shifts in the frequency distributions toward bigger values (**Figure** 4F-H, middle panels). We also observed the upward shift of the regression line describing the correlation between dendritic spine volume and PSD surface area in the WT Ext group, as compared to the WT 5US group (**Figure** 4I). Thus, in the WT group dendritic spines had relatively bigger PSDs after fear extinction than the dendritic spines of the same size in the 5US groups. Overall, the pattern of synaptic changes observed in the WT mice resembled the changes found in Thy1-GFP(M) animals after contextual fear extinction (**Figure** 1). The S73A mutation impaired fear extinction-induced downregulation of dendritic spine density as well as dendritic spine and PSD growth (**Figure** 4E-I). Altogether, our data indicate that PSD-95(S73) phosphorylation regulates both density and size of the excitatory synapses during contextual fear extinction.

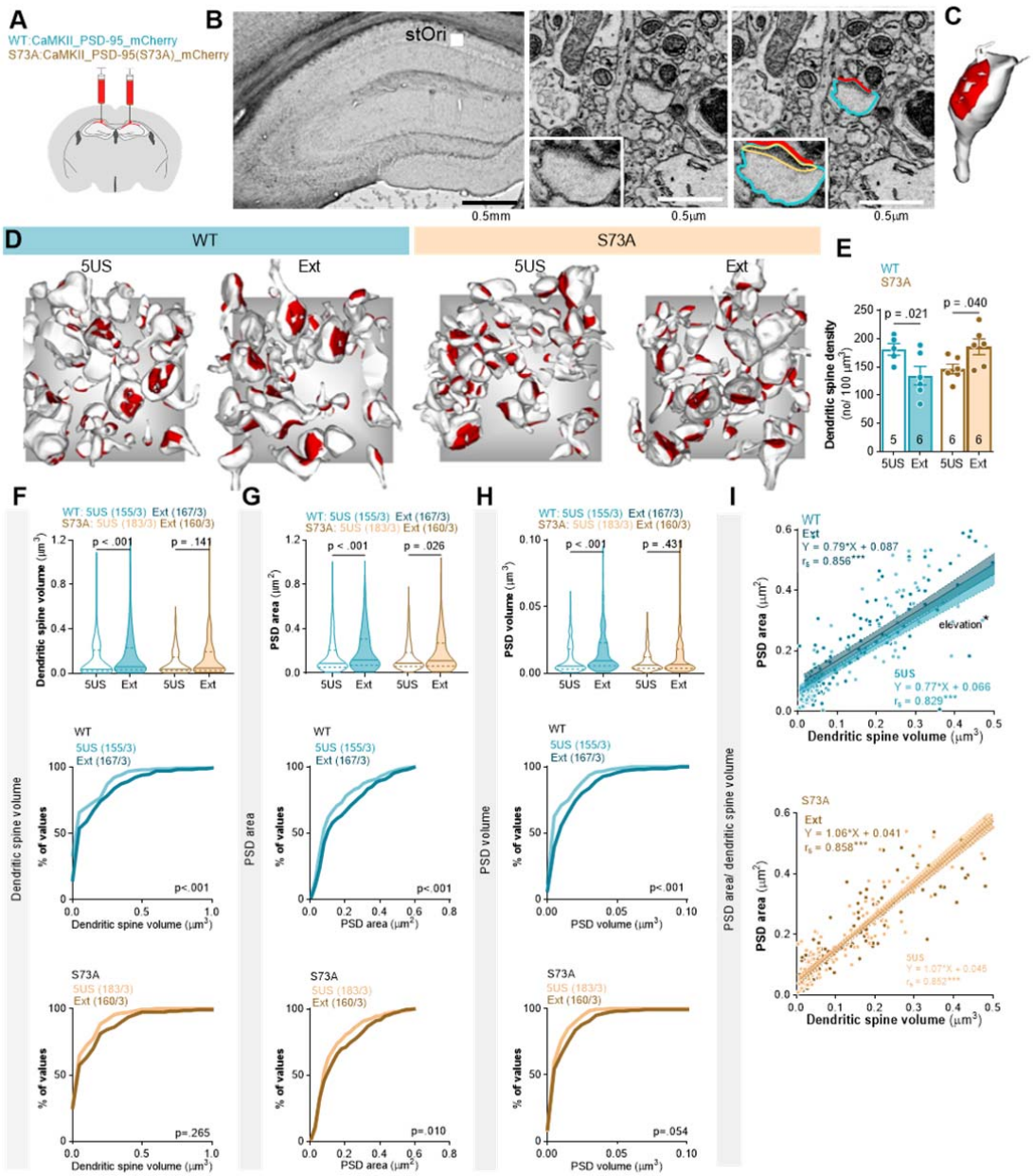

Figure 4. Phosphorylation of PSD-95(S73) regulates excitatory synapses during fear extinction.

(A) Male mice were stereotactically injected in the dCA1 with AAV1/2 encoding PSD-95(WT) (WT, n = 12) or PSD-95(S73A) (S73A, n = 12). Twenty one days later they underwent CFC and were sacrificed 1 day after training (5US) or they were re-exposed to the training context for fear extinction (Ext). **(B-C)** The principles for SBEM analysis of the ultrastructure of dendritic spines and PSDs. **(B, left)** Microphotography of a dorsal hippocampus with the region of interest for analysis and tracing of a dendritic spine and PSD in stOri. **(B, right)** A representative trace of a dendritic spine (blue), PSD surface area (red) and volume (yellow), and **(C)** reconstruction of this dendritic spine.

(D) Exemplary reconstructions of dendritic spines and their PSDs from SBEM scans in stOri. The grey background rectangles are x = 3 × y = 3 µm. Dendritic spines and PSDs were reconstructed and analysed in tissue bricks.

(E-I) Summary of data showing: **(E)** mean density of dendritic spines (two-way ANOVA with LSD *post hoc* tests for planned comparisons, effect of training: $F(1, 45) = 8.01$, $P = 0.007$); **(F)** median dendritic spine volume (Mann-Whitney test, WT: $U = 9766$, $P < 0.001$; S73A: $U = 13217$, $P = 0.141$) and distributions of dendritic spine volumes (numbers of the analysed dendritic spines/mice are indicated) (Kolmogorov-Smirnov test, WT: $D = 0.239$, $P < 0.001$; S73A: $D = 0.109$, $P = 0.265$); **(G)** median PSD surface area (Mann-Whitney test, WT: $U = 9948$, $P < 0.001$; S73A: $U = 46678$, $P = 0.024$) and distributions of PSD surface areas (numbers of the analysed dendritic spines/mice are indicated) (Kolmogorov-Smirnov test, WT: $D = 0.157$, $P < 0.001$; S73A: $D = 0.128$, $P = 0.010$); **(H)** median PSD volume (Mann-Whitney test, WT: $U = 9462$, $P < 0.001$; S73A: $U = 13621$, $P = 0.431$) and distributions of PSD volumes (numbers of the analysed dendritic spines/mice are indicated)(Kolmogorov-Smirnov test, WT: $D = 0.278$, $P < 0.001$; S73A: $D = 0.145$, $P = 0.054$); **(I)** correlation of dendritic spine volume and PSD surface area (ANCOVA, WT: elevation, $F(1, 319) = 4.256$, $P = 0.039$; S73A: elevation, $F(1, 340) = 0.603$, $P = 0.438$; linear regression equations and Spearman correlation R are given for raw data). For E, each dot represents one tissue brick and means ± SEM are shown; for F, G, H (top) medians ± IQR are shown; for I, each dot represents an individual dendritic spine and regression lines ± 95% confidence intervals are shown.

PSD-95(S73) phosphorylation in dCA1 is required for consolidation of contextual fear extinction memory.

To test whether phosphorylation of PSD-95(S73) is necessary for consolidation of fear extinction memory, we used dCA1-targeted expression of S73A, WT or control AAV1/2 encoding mCherry under *Camk2a* promoter (Control). Two cohorts of mice with dCA1-targeted expression of the Control virus, WT or S73A, underwent CFC and fear extinction training. The first cohort underwent a short extinction training with one 30-minute extinction session (Ext) and 5-minute test of fear extinction memory (Test) (**Figure** 5A), while the second underwent an extensive fear extinction training with three 30-minute contextual fear extinction sessions on the days 2, 3, 4 (Ext1-3), followed by spontaneous fear recovery/ remote fear memory test on day 18, and further three extinction sessions on the days 18-20 (Ext4-6). Next, fear generalisation was tested in a context B (CtxB, day 22) (**Figure** 5D). The post-training analysis showed that the viruses were expressed in dCA1 (**Figure** 5I-J). The control virus was expressed in 85% of the dCA1 cells, WT in 88% and S73A in 87% (**Figure** 5J).

The analysis of the short extinction training (data pooled from two cohorts) showed that in all experimental groups freezing levels were low at the beginning of the training and increased after 5US delivery (**Figure** 5B). Furthermore, mice in all groups showed high freezing levels at the beginning of the Ext indicating similar levels of contextual fear memory acquisition. However, freezing measured during the Test was significantly decreased, as compared to the beginning of Ext, only in the Control and WT groups, not in the S73A animals (**Figure** 5C).

The analysis of freezing levels during the extensive fear extinction training showed high levels of freezing at the end of training and beginning of Ext1 for all experimental groups (**Figure** 5E-F). In the Control and WT groups, the freezing levels decreased over consecutive extinction sessions (Ext2-6) and were significantly lower as compared to Ext1, indicating formation of long-term fear extinction memory. We also found no spontaneous fear recovery after 14-day delay (Ext4 vs Ext3; Control, P = 0.806; WT, P = 0.248). In the S73A group, the extensive contextual fear extinction protocol did not reduce freezing levels measured at the beginning of Ext6 sessions, as compared to Ext1, indicating no fear extinction (**Figure** 5F). Accordingly we found significantly larger reduction of freezing after fear extinction training (ΔExt6-Ext1) in the controls and WT animals, as compared to the S73A group (**Figure** 5G). The freezing reaction was specific for the training context, as it was very low and similar for all experimental groups in the context B (**Figure** 5H). Thus, our data indicate that expression of the S73A in dCA1 does not affect fear memory formation, recall or generalisation but prevents contextual fear extinction even after extensive fear extinction training.

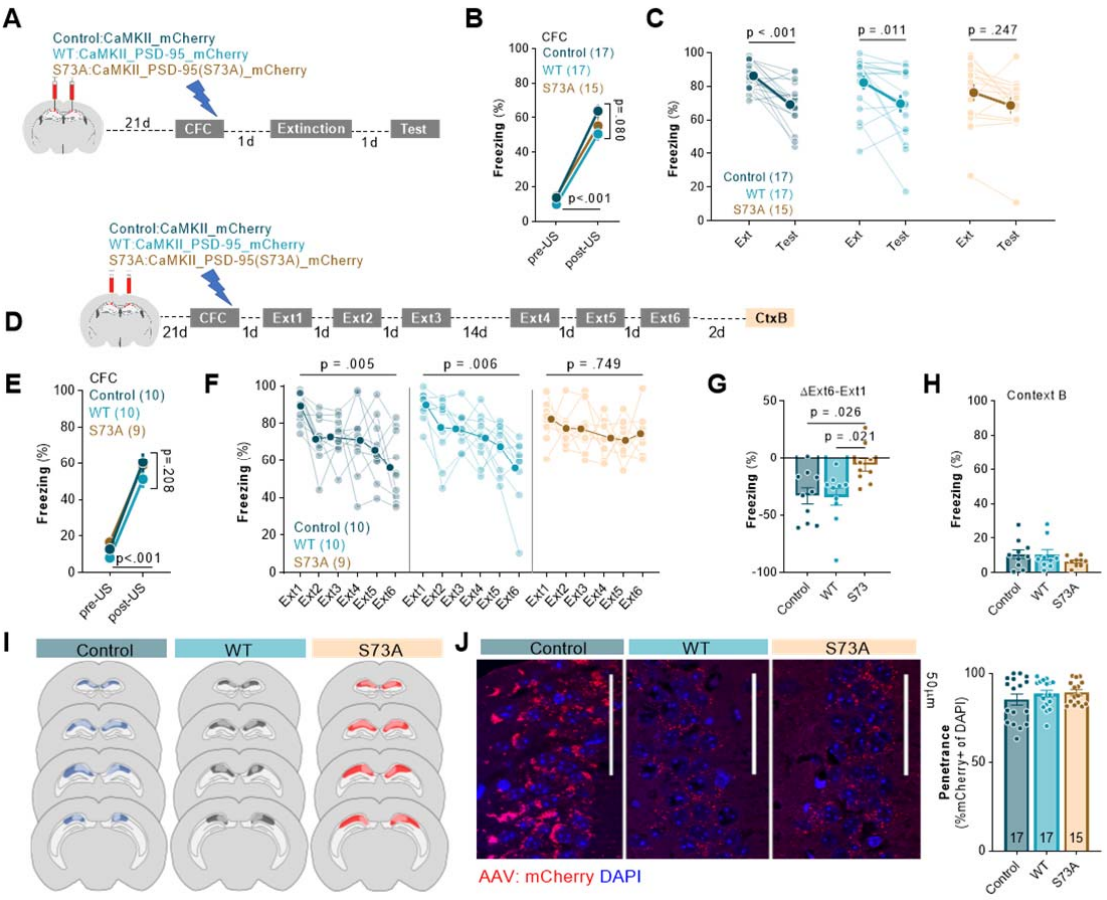

Figure 5. Phosphorylation of PSD-95(S73) in dCA1 is required for contextual fear extinction. (A)

Experimental timeline of the short fear extinction training. C57BL/6J male mice were stereotactically injected in the dCA1 with AAV1/2 encoding mCherry (Control, n = 17), PSD-95(WT) (WT, n = 17) or PSD-95(S73A) (S73A, n = 15). Twenty one days after surgery mice underwent CFC. One day after CFC they were re-exposed to the training context in the absence of foot shock (Extinction). Consolidation of fear extinction memory was tested one day later in the same context (Test).

(B-C) Summary of data showing percentage of freezing during **(B)** CFC, **(C)** Extinction and Test of the mice with dCA1-targeted expression of Control, WT or S73A (two-way repeated-measures ANOVA with Šídák's multiple comparisons test, effect of time: $F(1, 46) = 26.13$, $P < 0.001$, genotype: $F(2, 46) = 0.540$, $P = 0.586$; time x genotype: $F(2, 46) = 1.25$, $P = 0.296$).

(D) Experimental timeline of the extensive fear extinction training. Mice with dCA1-targeted expression of Control (n=10), WT (n=10) or S73A (n=9) underwent CFC, followed by six 30-min fear extinction sessions (Ext1-6) and one exposure to novel context without footshock (CtxB).

(E-H) Summary of data showing freezing levels **(E)** during CFC, **(F)** after extensive fear extinction training (two-way repeated-measures ANOVA with Dunnett's multiple comparisons test, effect of time: $F(3.681, 95.70) = 13.01$, $P < 0.001$; genotype: $F(2, 26) = 1.23$, $P = 0.306$; time x genotype: $F(10, 130) = 1.49$, $P = 0.147$), **(G)** the difference in freezing between Ext1 and Ext6 (one-way ANOVA with Tukey's multiple comparisons test, $F(2, 24.94) = 4.98$, $P = 0.016$), and **(H)** during the test in the context B (Brown-Forsythe ANOVA test, $F(2, 17.56) = 0.902$, $P = 0.428$).

(I) The extent of viral infection. **(J)** Single confocal scans of the stratum pyramidale of dCA1 of the mice expressing Control, WT and S73A and penetrance of the viruses. Means ± SEM are shown.

αCaMKII autophosphorylation regulates contextual fear extinction and PSD-95 protein levels during contextual fear extinction.

PSD-95(S73) is phosphorylated by αCaMKII (Gardoni et al., 2006; Steiner et al., 2008). To test the role of αCaMKII in PSD-95 protein regulation during fear extinction, autophosphorylation-deficient αCaMKII mutant mice (T286A) (Giese et al., 1998) and their wild-type (WT) littermates (males and females, in sex-balanced groups) were trained in CFC. They had similar and low levels of freezing in the novel context and freezing increased after 5US delivery (**Figure** 6A). Mice of both genotypes also showed high levels of freezing in the training context on the next day (Ext1), indicating contextual fear memory formation. However, when the mice were re-exposed to the training context for fear extinction (Ext2-3), the freezing levels of WT mice were significantly lower, as compared to Ext1, while the T286A mutants showed still high freezing . Thus, we confirmed that αCaMKII autophosphorylation is required for contextual fear memory extinction.

Next, a second cohort of WT and T286A mice was trained and the animals were sacrificed 24 hours after training (5US) or after fear extinction session (Ext). The total levels of PSD-95 were not affected by the fear extinction session in WT mice (**Figure** 6C). However, PSD-95 levels were higher in all strata of dCA1 in the T286A Extinction group, as compared to WT animals sacrificed after

extinction, and T286A mutants sacrificed before extinction . The density of PSD-95$^+$ puncta was decreased, while mean area of the puncta increased in stOri in the WT Ext animals as compared to the WT 5US mice (**Figure** 6D-E). Moreover, in the T286A Ext group the density of PSD-95$^+$ puncta was higher in all strata of dCA1, as compared to the WT Ext animals (**Figure** 6D). Thus, this experiment supports the hypothesis that αCaMKII autophosphorylation is required for extinction-induced regulation of PSD-95$^+$ density.

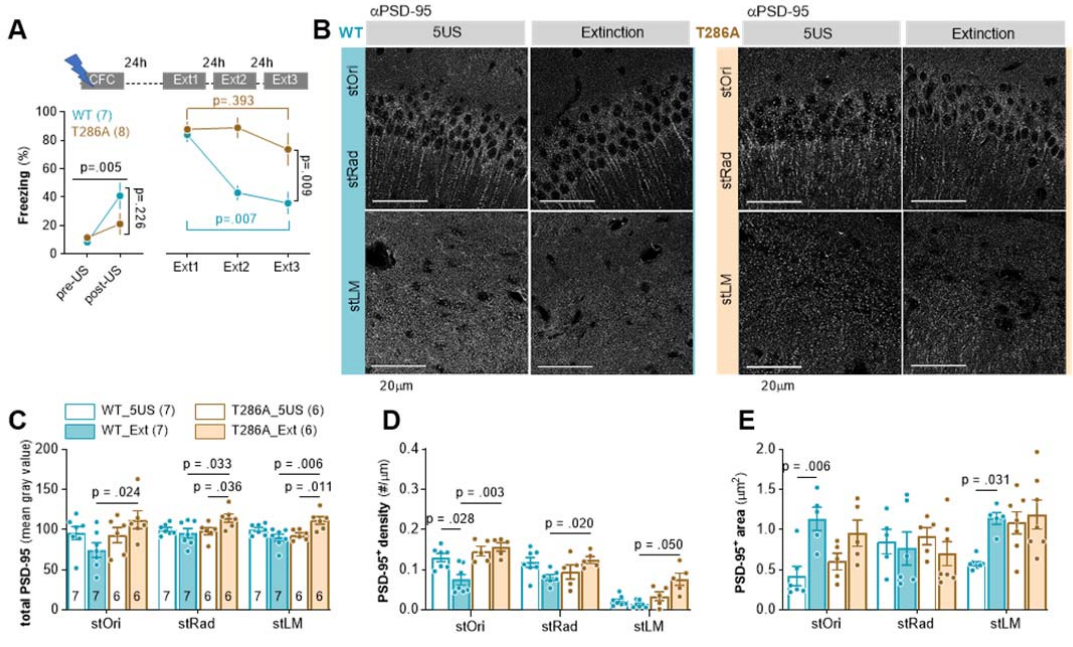

Figure 6. Autophosphorylation of αCaMKII is required for extinction of contextual fear and regulation of PSD-95 levels during fear extinction training.

(A) Experimental timeline [WT and T286A underwent CTC and three fear extinction sessions (Ext1-3)] and percentage of freezing during CFC (two-way repeated-measures ANOVA, effect of time: $F(1, 10) = 13.06$, $P = 0.005$; effect of genotype: $F(1, 10) = 1.66$, $P = 0.226$) and Ext1-3 (WT/T286A = 7/8; sex-balanced groups) (two-way repeated-measures ANOVA with Šídák's multiple comparisons test, effect of training: $F(1,430, 18,59) = 14.96$, $P < 0.001$; effect of genotype: $F(1, 13) = 9.30$, $P = 0.009$). **(B-E)** Analysis of PSD-95 expression in T286A mice.

(B) Representative confocal scans of the brain slices immunostained for PSD-95. **(C-E)** Quantification of the PSD-95 protein levels: **(C)** total PSD-95 levels (three-way repeated-measures ANOVA with with Tukey's *post hoc* test, effect of genotype x training: $F(1, 22) = 15.03$, $P < 0.001$); **(D)** density of PSD-95$^+$ puncta (three-way repeated-measures ANOVA with Tukey's *post hoc* test, effect of genotype x training: $F(1, 59) = 23.43$, $P < 0.001$); **(E)** area of PSD-95$^+$ puncta (three-way repeated-measures ANOVA with Tukey's *post hoc* test, effect of region x training: $F(2, 35) = 6.858$, $P = 0.003$). Mice: 5US/Ext, WT= 7/7; T286A = 6/6. Means ± SEM are shown.

DISCUSSION

We have investigated the role of dCA1 PSD-95(S73) phosphorylation in contextual fear extinction. Our study showed that: (1) contextual fear extinction induces transient changes of dCA1 PSD-95 protein levels and dendritic spines in a stratum-specific manner. The most pronounced changes are observed in stOri; (2) contextual fear extinction induces phosphorylation of PSD-95(S73) in all dCA1 strata; (3) Expression of the exogenous, phosphorylation-deficient PSD-95(S73A) in dCA1 deregulates PSD-95 protein levels and synaptic remodelling induced by extinction of fear memories; (4) dCA1 PSD-95(S73A) impaires long-term, contextual fear extinction memory, but not for fear memory formation or recall; (5) Phosphorylation-deficient αCaMKII(T286A) impairs contextual fear extinction and regulation of dCA1 PSD-95 protein levels during fear extinction.

Here, we demonstrate that contextual fear extinction transiently increases phospho-PSD-95(S73) levels and induces rapid downregulation of the synapses with PSD-95 as well as growth of the remaining synapses in stOri. These synaptic processes are homeostatic - without the changes of total PSD-95 levels and synaptic strength. Such synaptic plasticity alludes to the Hebbian strengthening of activated synapses and heterosynaptic weakening of adjacent synapses (Royer and Paré, 2003; El-Boustani et al., 2018). Our study is the first demonstration of the homeostatic plasticity of dendritic spines during attenuation of fear memories. We also show that extinction-induced downregulation of stOri synapses, as well as regulation of PSD-95 protein levels, are impaired by the expression of phosphorylation-deficient PSD-95(S73A). These observations indicate that phosphorylation of PSD-95(S73) is a key step in the regulation of the dCA1 circuit during fear extinction. There are several important limitations of our study. Firstly, using phospho-S73 antibody we cannot exclude that other MAGUKs are detected (due to the similar LERGN**S**GLGFS sequence). However, the role of phospho-PSD-95(S73) in contextual fear extinction is supported by the fact that there is increased colocalization of PSD-95 and phospho-S73 during extinction. Moreover, using *ex vivo* analyses we cannot unequivocally indicate whether PSD-95(S73A) prevents elimination of dendritic spines and PSD-95 proteins, or changes the balance of the synapses by enhancing synaptogenesis and protein synthesis. We believe, however, that the first scenario is more likely and this conclusion is supported by several observations. Firstly, PSD-95(S73A) does not affect synaptic strengthening (Steiner et al., 2008), but PSD-95(S73) phosphorylation allows for dissociation of PSD-95 from the complex with GluN2A, destabilisation of PSD and termination of synaptic growth after NMDAR stimulation (Gardoni et al., 2006; Steiner et al., 2008) as well as downregulation of PSD-95

levels during NMDAR-LTD (Nowacka et al., 2020). Secondly, both dCA1 phosphorylation of PSD-95(S73) and protein degradation, but not protein synthesis, are necessary for contextual fear extinction (Fischer, 2004; Lee et al., 2008).

Our experiments are the first to show that phosphorylation of PSD-95(S73) in dCA1 is required for extinction of contextual fear memories. Strikingly, the contextual fear memory cannot be updated even when the animals with dCA1 PSD-95(S73A) mutation undergo six 30-minute extinction sessions. We also show that dCA1 PSD-95(S73A) does not affect mice activity, long-term fear memory formation and recall, context-independent fear generalisation or fear recovery after 14-day delay, pointing towards engagement of PSD-95(S73) phosphorylation only during extinction of contextual fear. This conclusion seemingly contradicts the study demonstrating that ligand binding-deficient PSD-95 knockin mice have enhanced contextual fear memory formation and impaired long-term memory retention (Nagura et al., 2012; Fitzgerald et al., 2015). However, even though the behavioural phenotype of PSD-95 KI mice was supported by LTP analysis in dCA1 (Nagura et al., 2012; Fitzgerald et al., 2015), it is unknown whether the mouse phenotype relies on the CA1 plasticity as the mutation was global. Furthermore, it is possible that PSD-95 KI and PSD-95(S73A) impact different stages of contextual fear memory. In agreement with our findings, the signalling pathways downstream of NMDAR-PSD-95 complex in the dorsal CA3 and DG regulate contextual fear extinction (Li et al., 2017; Cai et al., 2018). In particular, translocation of PSD-95 from NMDAR to TrkB, and increased PSD-95-TrkB interactions, promote extinction, while competing NMDAR-PSD-95-nNOS interactions hinder contextual fear extinction (Cai et al., 2018). Since PSD-95(S73A) mutation prolongs NMDAR-PSD-95 interactions (Gardoni et al., 2006) it may limit interactions of PSD-95 with TrkB and fear extinction. To support this hypothesis we also show that autophosphorylation of αCaMKII, the key enzyme activated by NMDAR, is required for extinction-induced regulation of PSD-95 levels and fear extinction.

Our data show that the extinction of contextual fear affects PSD-95 protein levels and dendritic spines predominantly in the stOri. This indicates that the extinction-induced synaptic remodelling is strikingly different from the changes observed immediately after contextual fear memory encoding where transient synaptogenesis is observed in the stRad (Radwanska et al., 2011). These observations support the idea that different CA1 inputs are involved in memory formation and extinction. CA3 neurons project to the stRad and stOri regions of CA1 pyramidal neurons, the nucleus

reuniens (Re) projects to the stOri and stLM, and the entorhinal cortex (EC) projects to the stLM (Ishizuka et al., 1990; Kajiwara et al., 2008; Hoover and Vertes, 2012; Vertes et al., 2015). Thus, the pattern of synaptic changes induced by contextual fear extinction co-localises with the domains innervated by the Re and EC, suggesting that these inputs are regulated during contextual fear extinction. In agreement with our observations, previous data showed that the EC is activated during and required for contextual fear extinction in animal models (Bevilaqua et al., 2006; Baldi and Bucherelli, 2015). Human studies also showed that EC-CA1 projections are activated by cognitive prediction error (that may drive memory extinction), while CA3-CA1 projections are activated by memory recall without prediction errors (Bein et al., 2020). The role of the Re in fear memory encoding, retrieval, extinction and generalisation has been demonstrated (Xu and Sudhof, 2013; Ramanathan et al., 2018; Troyner and Bertoglio, 2021). Still, it has to be established whether the plasticity of dCA1 synapses is specific to Re and/or EC projections.

Our findings add up to the previous studies investigating the molecular processes in dCA1 that are specific and required for contextual fear extinction, but not for fear memory consolidation, including regulation of ERK, CB1, and CBEP (Berger-Sweeney et al., 2006; Bitencourt et al., 2008; de Oliveira Alvares et al., 2008; Pamplona et al., 2008; Tronson et al., 2009; Radulovic and Tronson, 2010). Interestingly, other processes, such as protein synthesis and c-Fos expression, are necessary for contextual fear consolidation and reconsolidation, but not extinction (Fischer, 2004; Lattal and Abel, 2004; Mamiya et al., 2009; Tronson et al., 2009). Thus, although it is not surprising that distinct molecular cascades and cell circuits contribute to fear memory formation/recall and extinction (Tronson et al., 2009; Lacagnina et al., 2019), it remains puzzling how synaptic plasticity, without concomitant translation, contributes to contextual fear extinction. This observation points towards the role of protein synthesis-independent short-term plasticity, or protein degradation (Lee et al., 2008), in contextual fear extinction memory. The role of short-term plasticity in contextual fear extinction is supported by the observations that PSD-95(S73) phosphorylation and synaptic remodelling induced by fear extinction are transient. Similar short plasticity was observed by other groups upon recall of drug-paired memories (Gipson et al., 2013a, 2013b). Still it has to be clarified in the future studies how short-term dCA1 plasticity can support long-term fear extinction memory.

Conclusions

Our study demonstrates that extinction of contextual fear memories relies on rapid and transient synaptic plasticity in dCA1 that requires PSD-95(S73) phosphorylation. Thus our study supports the hypothesis that NMDAR-dependent plasticity in dCA1 is required to detect and resolve contradictory or ambiguous memories when spatial information is involved (Bannerman et al., 2014), the comparator view of hippocampal function (Gray, 1982; Grossberg and Merrill, 1992) as well as the observations that the hippocampus processes surprising events and prediction errors (Ploghaus et al., 2000; Kumaran and Maguire, 2006; Huh et al., 2009; Bein et al., 2020). Since new or long-lasting memories may be repeatedly reorganised upon recall (Nader et al., 2000; Schafe et al., 2001), the molecular and cellular mechanisms involved in extinction of the existing fearful memories provide excellent targets for fear memory impairment therapies. In particular, understanding the mechanisms that underlie contextual fear extinction may be relevant for post-traumatic stress disorder treatment.

Acknowledgments, Funding and Disclosure

This work was supported by a National Science Centre (Poland) Grant No. 2015/19/B/NZ4/02996 and 2020/38/A/NZ4/00483 to KR. PRELUDIUM Grant No. 2016/21/N/NZ4/03304 to MZ and PRELUDIUM Grant No. 2015/19/N/NZ4/03611 to KŁ. TW was supported by the National Science Centre (Poland) (Grant No. 2017/26/E/NZ4/00637). The project was carried out using CePT infrastructure financed by the European Union - The European Regional Development Fund within the Operational Program "Innovative economy" for 2007-2013.

MZ, MB, KFT and KR designed the experiments; MZ, MB, AC, MNS, AN, MŚ, KŁ, KFT, TW and AS performed the experiments; MZ, MB, MŚ, KŁ, ES, KFT, JW, TB and KR analysed data. MZ, MB and KR drafted the manuscript. All authors had critical input to the final version of the manuscript. Authors report no financial interests or conflicts of interest. Light and electron microscopy experiments were performed at the Laboratory of Imaging Tissue Structure and Functions, Nencki Institute.

MATERIALS AND METHODS

Animals. C57BL/6J male mice were purchased from Białystok University, Poland. Thy1-GFP(M) (The Jackson Laboratory, JAX:007788, RRID:IMSR_JAX:007788) mutant mice were bred as heterozygotes at Nencki Institute, and PCR genotyped as previously described (Feng et al., 2000). αCaMKII-T286A mutant mice were bred as heterozygotes at Nencki Institute, and PCR genotyped as previously described (Giese et al., 1998). All mice in the experiments were 10-week old at the beginning of the experiments. The mice were housed in groups of two to six and maintained on a 12 h light/dark cycle with food and water *ad libitum*. All experiments with transgenic mice used approximately equal numbers of males and females. The experiments were undertaken according to the Animal Protection Act of Poland and approved by the I Local Ethics Committee (261/2012 and 829/2019 Warsaw, Poland).

Contextual fear conditioning (CFC). The animals were trained in a conditioning chamber (Med Associates Inc, St Albans, USA) in a soundproof box. The chamber floor had a stainless steel grid for shock delivery. Before training, the chamber was cleaned with 70% ethanol, and a paper towel soaked in ethanol was placed under the grid floor. To camouflage background noise in the behavioural room, a white noise generator was placed inside the soundproof box.

On the conditioning day, the mice were brought from the housing room into a holding room to acclimatise for 30 min before training. Next, mice were placed in the training chamber, and after a 148 s introductory period, a foot shock (2 s, 0.7 mA) was presented. The shock was repeated 5 times, at 90 s inter-trial intervals. Thirty seconds after the last shock, the mouse was returned to its home cage. Contextual fear memory was tested and extinguished 24 h after training by re-exposing mice to the conditioning chamber for 30 minutes without US presentation, followed by the second 5-minute test session on the following day. During extensive contextual fear extinction, 30-minute fear extinction sessions were repeated on days 2, 3, 14, 15, and 16. Moreover mice activity and freezing were tested in context B (Ctx B) on day 17. A video camera was fixed inside the door of the sound attenuating box for the behavior to be recorded and scored. Freezing behavior (defined as complete lack of movement, except respiration) and locomotor activity of mice were automatically scored. The experimenters were blind to the experimental groups.

Stereotactic surgery. Mice were fixed in a stereotactic frame (51503, Stoelting, Wood Dale, IL, USA) and kept under isoflurane anesthesia (5% for induction, 1.5-2.0% during surgery). Adeno-associated viruses, serotype 1 and 2, (AAV1/2), solutions were injected into the dorsal CA1 area (Paxinos & Franklin 2001) at coordinates in relation to Bregma (AP, -2.1mm; ML, ±1.1 mm; DV, -1.3mm). 450 nl of AAV solutions were injected into the CA1 through a beveled 26 gauge metal needle, and 10 µl microsyringe (SGE010RNS, WPI, USA) connected to a pump (UMP3, WPI, Sarasota, USA), and its controller (Micro4, WPI, Sarasota, USA) at a rate 50 nl/ min. The needle was then left in place for 5 min, retracted +100 nm DV, and left for an additional 5 min to prevent unwanted spread of the AAV solution. Titers of AAV1/2 were: αCaMKII_PSD-95(WT):mCherry (PSD-95(WT)): 1.35 $x10^9$/µl, αCaMKII_PSD-95(S73A):mCherry (PSD-95(S73A)): 9.12 $x10^9$/µl), αCaMKII_mCherry (mCherry): viral titer 7.5 $x10^7$/µl (obtained from Karl Deisseroth's Lab). Mice were allowed to recover from anaesthesia for 2-3 h on a heating pad and then transferred to individual cages where they stayed until complete skin healing, and next, they were returned to the home cages. The viruses were prepared at the Nencki Institute core facility, Laboratory of Animal Models. After training, the animals were perfused with 4% PFA in PBS and bain sections from the dorsal hippocampus were immunostained for PSD-95 and imaged with Zeiss Spinning Disc confocal microscope (magnification: 10x) to assess the extent of the viral expression and PSD-95 expression.

Immunostaining. Mice were anaesthetised and perfused with cold phosphate buffer pH 7.4, followed by 0.5% 4% PFA in phosphate buffer. Brains were removed and postfixed o/n in 4°C. Brains were kept in 30% sucrose in PBS for 72h. Coronal brain sections were prepared using cryosectioning (40 µm thick, Cryostat CM1950, Leica Biosystems Nussloch GmbH, Wetzlar, Germany) and stored in a cryoprotecting solution in –20°C (PBS, 15% sucrose (Sigma-Aldrich), 30% ethylene glycol (Sigma-Aldrich), and 0.05% NaN_3 (SigmaAldrich). Before staining, sections were washed 3 × PBS and blocked for 1 hour at room temperature (RT) in 5% NDS with 0.3% Triton X-100 in PBS and then incubated o/n, 4°C with PSD-95 primary antibodies (1:500, Millipore, MAB1598, RRID:AB_11212185) and/or rabbit anti-mCherry primary antibodies (1:500, Abcam, ab167453, RRID:AB_2571870) and/or rabbit P-Ser73_PSD-95 primary antibodies (1:12, Davids Biotechnology, A061). On the second day slices were washed 3 × PBS with 0,3% Trition X-100 and incubated for 90 minutes with secondary antibodies conjugated with anti-mouse AlexaFluor 555 (1:500, Invitrogen, A31570, RRID:AB_2536180) and/or anti-rabbit AlexaFluor 555 (1:500, Invitrogen, A31572, RRID:AB_162543)

and/or anti-rabbit Alexa Fluor 647 (1:500, Invitrogen, A31573, RRID:AB_2536183). Slices were then mounted on microscope slides (Thermo Fisher Scientific) and covered with coverslips in Fluoromount-G medium with DAPI (00-4959-52, Invitrogen).

Phospho-PSD-95(S73)-specific antibody. Phospho-epitope-specific serum against phosphorylated PSD-95(S73) was raised in a rabbit using the synthetic phosphopeptide LERGN(Sp)GLGFS. The antibody was prepared and affinity-purified by Davids Biotechnologie (Regensburg, Germany).

Confocal microscopy and image quantification. The microphotographs of dendritic spines in the Thy1-GFP(M) mice, fluorescent PSD-95 and phospho-PSD-95(S73) immunostaining were taken on a Spinning Disc confocal microscope (63 × oil objective, NA 1.4, pixel size 0.13 µm × 0.13 µm) (Zeiss, Göttingen, Germany). We took microphotographs (16 bit, z-stacks of 12-48 scans; 260 nm z-steps) of 6 dendrites per region per animal from stratum oriens (stOri), stratum radiatum (stRad) and stratum lacunosum-moleculare (stLM) (in the middle of the strata) of dCA1 pyramidal neurons (AP, Bregma from -1.7 to 2.06). The PSD-95 fluorescent immunostaining after AAV overexpression was analysed with Zeiss LSM 800 microscope equipped with Airy-Scan detection (63× oil objective and NA 1.4, pixel size 0.13 µm × 0.13 µm, 8 bit) (Zeiss, Göttingen, Germany). A series of 18 continuous optical sections (67.72 µm × 67.72 µm), at 0.26 µm intervals, were scanned along the z-axis of the tissue section. Six to eight z-stacks of microphotographs were taken per animal per region, from every sixth section through dCA1. Each dendritic spine was manually outlined, and the spine area was measured with ImageJ 1.52n software measure tool. Custom-written Python scripts were used to analyse the mean grey value of PSD-95^{+} puncta per dendritic spine, total PSD-95 levels (as an image mean gray value), and PSD-95^{+} puncta density and size.

Serial Face-block Scanning Electron Microscopy (SBEM). Mice were transcardially perfused with cold phosphate buffer pH 7.4, followed by 0.5% EM-grade glutaraldehyde (G5882 Sigma-Aldrich) with 2% PFA in phosphate buffer pH 7.4 and postfixed overnight in the same solution. Brains were then taken out of the fixative and cut on a vibratome (Leica VT 1200) into 100 µm slices. Slices were kept in phosphate buffer pH 7.4, with 0.1% sodium azide in 4°C. For AAV-injected animals, the fluorescence of exogenous proteins was confirmed in all slices by fluorescent imaging. Then, slices were washed 3 times in cold phosphate buffer and postfixed with a solution of 2% osmium tetroxide (#75632 Sigma-Aldrich) and 1.5 % potassium ferrocyanide (P3289 Sigma-Aldrich) in 0.1 M phosphate buffer pH 7.4

for 60 min on ice. Next, samples were rinsed 5 × 3 min with double distilled water (ddH_2O) and subsequently exposed to 1% aqueous thiocarbohydrazide (TCH) (#88535 Sigma) solution for 20 min. Samples were then washed 5 × 3 min with ddH_2O and stained with osmium tetroxide (1% osmium tetroxide in ddH_2O, without ferrocyanide) for 30 min in RT. Afterward, slices were rinsed 5 × 3 min with ddH_2O and incubated in 1% aqueous solution of uranium acetate overnight in 4°C. The next day, slices were rinsed 5 × 3 min with ddH_2O, incubated with lead aspartate solution (prepared by dissolving lead nitrate in L-aspartic acid as previously described (Deerinck et al., 2010)) for 30 min in 60°C and then washed 5 × 3 min with ddH_2O and dehydration was performed using graded dilutions of ice-cold ethanol (30%, 50%, 70%, 80%, 90%, and 2 × 100% ethanol, 5 min each). Then slices were infiltrated with Durcupan resin. A(17 g), B(17 g) and D(0,51 g) components of Durcupan (#44610 Sigma-Aldrich) were first mixed on a magnetic stirrer for 30 min and then 8 drops of DMP-30 accelerator (#45348 Sigma) were added (Knott et al., 2009). Part of the resin was then mixed 1:1 (v/v) with 100% ethanol and slices were incubated in this 50% resin on a clock-like stirrer for 30 min in RT. The resin was then replaced with 100% Durcupan for 1 hour in RT and then 100% Durcupan infiltration was performed o/n with constant slow mixing. The next day, samples were infiltrated with freshly prepared resin (as described above) for another 2 hours in RT, and then embedded between flat Aclar sheets (Ted Pella #10501-10). Samples were put in a laboratory oven for at least 48 hours at 65°C for the resin to polymerize. After the resin hardened, the Aclar layers were separated from the resin embedded samples, dCA1 region was cut out with a razorblade. Caution was taken for the piece to contain minimal resin. Squares of approximately 1 × 1 × 1 mm were attached to aluminium pins (Gatan metal rivets, Oxford instruments) with very little amount of cyanacrylamide glue. After the glue dried, samples were mounted to the ultramicrotome to cut 1 µm thick slices. Slices were transferred on a microscope slide, briefly stained with 1% toluidine blue in 5% borate and observed under a light microscope to confirm the region of interest (ROI). Next, samples were grounded with silver paint (Ted Pella, 16062-15) and pinned for drying for 4 – 12 hours, before the specimens were mounted into the 3View2 chamber.

SBEM *imaging and 3D reconstructions.* Samples were imaged with Zeiss SigmaVP (Zeiss, Oberkochen, Germany) scanning electron microscope equipped with 3View2 chamber using a backscatter electron detector. Scans were taken in the middle portion of dCA1 stOri. From each sample, 200 sections were collected (thickness 60 nm). Imaging settings: high vacuum with EHT 2.9-

3.8 kV, aperture: 20 µm, pixel dwell time: 3 µs, pixel size: 5 – 6.2 nm. Scans were aligned using the ImageJ software (ImageJ -> Plugins -> Registration -> StackReg) and saved as .tiff image sequence. Next, aligned scans were imported to Reconstruct software (Fiala 2005), available at http://synapses.clm.utexas.edu/tools/reconstruct/reconstruct.stm (Synapse Web Reconstruct, RRID:SCR_002716). Dendritic spine density was analysed from 3 bricks per animal with the unbiased brick method (Fiala and Harris 2001) per tissue volume. Brick dimensions 3 × 3 × 3 µm were chosen to exceed the length of the largest profiles in the data sets at least twice. To calculate the density of dendritic spines, the total volume of large tissue discontinuities was subtracted from the volume of the brick. The density of dendritic spines was normalised to AAV1/2 penetrance.

A structure was considered to be a dendritic spine when it was a definite protrusion from the dendrite, with electron-dense material (representing postsynaptic part of the synapse, PSD) on the part of the membrane that opposed an axonal bouton with at least 3 vesicles within a 50-nm distance from the cellular membrane facing the spine. For 3D reconstructions, PSDs and dendritic spines in one brick were reconstructed for each sample. PSDs were first reconstructed and second, their dendritic spines were outlined. To separate dendritic spine necks from the dendrites, a cut-off plane was used approximating where the dendritic surface would be without the dendritic spine. PSD volume was measured by outlining dark, electron-dense area on each PSD containing section (Borczyk et al., 2019). The PSD area was measured manually according to the Reconstruct manual. All non-synaptic protrusions were omitted in this analysis. For multi-synaptic spines, the PSD areas and volumes were summed.

Correlative light-electron microscopy (CLEM). CLEM workflow was based on a previously established protocol with some modifications (Bishop et al., 2011). Mice infused with PSD-95(WT) in the CA1 were perfused as described above. Brains were then removed and postfixed o/n in 4°C. 100 µm thick brain slices were cut on a vibratome and embedded in low melting point agarose in phosphate buffer and mounted into imaging chambers. mCherry fluorescence in the stRad was photographed using Zeiss LSM800, z-stacks of 60 images (60 µm thick) at 63 × magnification. Next, the slice was transferred under the 2P microscope (Zeiss MP PA Setup), where a Chameleon laser was used to brand mark the ROI (laser length 870 nm, laser power 85%, 250 scans of each line). Then, SBEM staining was performed as described above. The resin-embedded hippocampus was then divided into 4 rectangles and each was mounted onto metal pins to locate the laser-induced marks. SBEM scanned within the

662 laser marked frame. The fluorescent image was overlaid onto the SBEM image using dendrites and
663 cell nuclei as landmarks using ImageJ 1.48k software (RRID:SCR_003070).

664 *Electrophysiology.* Mice were deeply anaesthetised with Isoflurane, decapitated and the brains were
665 rapidly dissected and transferred into ice-cold cutting artificial cerebrospinal fluid (ACSF) consisting of
666 (in mM): 87 NaCl, 2.5 KCl, 1.25 NaH2PO4, 25 NaHCO3, 0.5 CaCl2, 7 MgSO4, 20 D-glucose, 75
667 sacharose equilibrated with carbogen (5% CO2/95% O2). The brain was cut to two hemispheres and
668 350 µm thick coronal brain slices were cut in ice-cold cutting ACSF with Leica VT1000S vibratome.
669 Slices were then incubated for 15 min in cutting ACSF at 32°C. Next the slices were transferred to
670 recording ACSF containing (in mM): 125 NaCl, 2.5 KCl, 1.25 NaH_2PO_4, 25 $NaHCO_3$, 2.5 $CaCl_2$, 1.5
671 $MgSO_4$, 20 D-glucose equilibrated with carbogen and incubated for minimum 1 hour at room
672 temperature (RT).

673 Extracellular field potential recordings were recorded in a submerged chamber perfused with
674 recording ACSF in RT. The synaptic potentials were evoked with a Stimulus Isolator (A.M.P.I Isoflex)
675 with a concentric bipolar electrode (FHC, CBARC75) placed in the stOri of CA2 on the experiment.
676 The stimulating pulses were delivered at 0.1 Hz and the pulse duration was 0.3 ms. Recording
677 electrodes (resistance 1-4 MΩ) were pulled from borosilicate glass (WPI, 1B120F-4) with a
678 micropipette puller (Sutter Instruments, P-1000) and filled with recording ACSF. The recording
679 electrodes were placed in stOri of dCA1. Simultaneously, a second recording electrode was placed in
680 the stratum pyramidale to measure population spikes. For each slice, the recordings were done in
681 stOri. Recordings were acquired with MultiClamp 700B amplifier (Molecular Devices, California, USA),
682 digitised with Digidata 1550B (Molecular Devices, California, USA) and pClamp 10.7 Clampex 10.0
683 software (Molecular Devices, California, USA). Input/output curves were obtained by increasing
684 stimulation intensity by 25 µA in the range of 0-300 µA. All electrophysiological data were analysed
685 with AxoGraph 1.7.4 software (Axon Instruments, U.S.A). The amplitude of fEPSP, relative amplitude
686 of population spikes and fibre volley were measured.

687 *Statistics.* Data are presented as mean ± standard error of the mean (SEM) for populations with
688 normal distribution or as median ± interquartile range (IQR) for populations with non-normal
689 distribution. An animal was used as a biological replication in all experiments except for the dendritic
690 spine size distribution analysis. When the data met the assumptions of parametric statistical tests,

691 results were analysed by one- or repeated measures two-way ANOVA, followed by Tukey's or Fisher's
692 *post hoc* tests, where applicable. Data were tested for normality by using the Shapiro-Wilk test of
693 normality and for homogeneity of variances by using the Levene's test. For repeated-measure data
694 with missing observation, a linear mixed model was used to analyse the results, followed by pairwise
695 comparisons with Sidak adjustment for multiple comparisons. Areas of dendritic spines and PSDs did
696 not follow normal distributions and were analysed with the Kruskal-Wallis test. Frequency distributions
697 of PSD area to the spine volume ratio were compared with the Kolmogorov-Smirnov test. Correlations
698 were analysed using Spearman correlation (Spearman r (s_r) is shown), and the difference between
699 slopes or elevation between linear regression lines was calculated with ANCOVA. Differences
700 between the experimental groups were considered statistically significant if $P < 0.05$. Analyses were
701 performed using the Graphpad Prism 9. Mice were excluded from the analysis only if they did not
702 express the tested virus in the target region.

703

Key Resources Table				
Reagent type (species) or resource	**Designation**	**Source or reference**	**Identifiers**	**Additional information**
strain, strain background (*Mus musculus,* male)	Thy1-GFP(M)	**PMID: 11086982**		
strain, strain background (*Mus musculus,* male)	C57BL/6J	Białystok University, Poland	IMSR_JAX:007788	
antibody	mouse PSD-95 primary antibody	Millipore MAB1598	RRID:AB_11212185	1:500
antibody	rabbit P-Ser73_PSD-95 primary antibody	Davids Biotechnologie	A061	1:12
antibody	Donkey anti-Mouse IgG alexa fluor 555	Invitrogen A31570	RRID:AB_2536180	1:500

Key Resources Table				
antibody	Rabbit anti-mCherry	Abcam, ab167453	RRID:AB_2571870	1:500
antibody	Donkey anti-rabbit Alexa Fluor 555	Invitrogen,A-31572	RRID:AB_162543	1:500
antibody	Donkey anti-rabbit Alexa Fluor 647	Invitrogen, A31573	RRID:AB_2536183	1:500
recombinant DNA reagent	AAV1/2, *Camk2a*_PSD-95(WT):mCherry (PSD-95(WT))	PMID: **32029829**		*Dlg4* cloned into Addgene plasmid # 114469
recombinant DNA reagent	AAV1/2, *Camk2a*_PSD-95(S73A):mCherry (PSD-95(S73A))	PMID: **32029829**		*Dlg4*_S73A cloned into Addgene plasmid # 114469
recombinant DNA reagent	AAV1/2, *Camk2a*_mCherry (mCherry)	Addgene plasmid # 114469	RRID:Addgene_114469	
software, algorithm	ImageJ (Fiji)	PMID: 22743772	RRID:SCR_002285	
software, algorithm	Med-PC V Software Suite	Med Associate Inc.	SOF-736	fear conditioning software
software, algorithm	Reconstruct	PMID: **15817063**	RRID:SCR_002716	

704

705

706 **REFERENCES**

707 Abraham WC, Jones OD, Glanzman DL (2019) Is plasticity of synapses the mechanism of long-term
708 memory storage? Npj Sci Learn 4:9 Available at: http://www.nature.com/articles/s41539-019-
709 0048-y [Accessed November 4, 2020].
710 Aziz W, Kraev I, Mizuno K, Kirby A, Fang T, Rupawala H, Kasbi K, Rothe S, Jozsa F, Rosenblum K,
711 Stewart MG, Giese KP (2019) Multi-input Synapses, but Not LTP-Strengthened Synapses,
712 Correlate with Hippocampal Memory Storage in Aged Mice. Curr Biol 29:3600-3610.e4
713 Available at: https://linkinghub.elsevier.com/retrieve/pii/S0960982219311145 [Accessed
714 November 3, 2020].
715 Baldi E, Bucherelli C (2015) Brain sites involved in fear memory reconsolidation and extinction of
716 rodents. Neurosci Biobehav Rev 53:160–190 Available at:
717 https://linkinghub.elsevier.com/retrieve/pii/S0149763415000998 [Accessed November 3,
718 2020].
719 Bannerman DM, Bus T, Taylor A, Sanderson DJ, Schwarz I, Jensen V, Hvalby Ø, Rawlins JNP,
720 Seeburg PH, Sprengel R (2012) Dissecting spatial knowledge from spatial choice by
721 hippocampal NMDA receptor deletion. Nat Neurosci 15:1153–1159 Available at:
722 http://www.nature.com/articles/nn.3166 [Accessed November 3, 2020].
723 Bannerman DM, Sprengel R, Sanderson DJ, McHugh SB, Rawlins JNP, Monyer H, Seeburg PH
724 (2014) Hippocampal synaptic plasticity, spatial memory and anxiety. Nat Rev Neurosci
725 15:181–192 Available at: https://www.nature.com/articles/nrn3677 [Accessed January 25,
726 2021].
727 Bats C, Groc L, Choquet D (2007) The Interaction between Stargazin and PSD-95 Regulates AMPA
728 Receptor Surface Trafficking. Neuron 53:719–734 Available at:
729 https://www.sciencedirect.com/science/article/pii/S0896627307000712 [Accessed April 15,
730 2021].
731 Bein O, Duncan K, Davachi L (2020) Mnemonic prediction errors bias hippocampal states. Nat
732 Commun 11:3451 Available at: http://www.nature.com/articles/s41467-020-17287-1
733 [Accessed November 4, 2020].
734 Béïque J, Andrade R (2003) PSD□95 regulates synaptic transmission and plasticity in rat cerebral
735 cortex. J Physiol 546:859–867 Available at:
736 https://onlinelibrary.wiley.com/doi/10.1113/jphysiol.2002.031369 [Accessed November 3,
737 2020].
738 Berger-Sweeney J, Zearfoss NR, Richter JD (2006) Reduced extinction of hippocampal-dependent
739 memories in CPEB knockout mice. Learn Mem Cold Spring Harb N 13:4–7.
740 Bevilaqua L, Bonini J, Rossato J, Izquierdo L, Cammarota M, Izquierdo I (2006) The entorhinal cortex
741 plays a role in extinction. Neurobiol Learn Mem 85:192–197 Available at:
742 https://linkinghub.elsevier.com/retrieve/pii/S1074742705001073 [Accessed November 4,
743 2020].
744 Bitencourt RM, Pamplona FA, Takahashi RN (2008) Facilitation of contextual fear memory extinction
745 and anti-anxiogenic effects of AM404 and cannabidiol in conditioned rats. Eur
746 Neuropsychopharmacol J Eur Coll Neuropsychopharmacol 18:849–859.
747 Bliss TVP, Collingridge GL (1993) A synaptic model of memory: long-term potentiation in the
748 hippocampus. Nature 361:31–39 Available at: https://www.nature.com/articles/361031a0
749 [Accessed July 29, 2021].
750 Borczyk M, Śliwińska MA, Caly A, Bernas T, Radwanska K (2019) Neuronal plasticity affects
751 correlation between the size of dendritic spine and its postsynaptic density. Sci Rep 9:1693
752 Available at: http://www.nature.com/articles/s41598-018-38412-7 [Accessed November 3,
753 2020].
754 Cai C-Y, Chen C, Zhou Y, Han Z, Qin C, Cao B, Tao Y, Bian X-L, Lin Y-H, Chang L, Wu H-Y, Luo C-X,
755 Zhu D-Y (2018) PSD-95-nNOS Coupling Regulates Contextual Fear Extinction in the Dorsal
756 CA3. Sci Rep 8:12775 Available at: https://www.nature.com/articles/s41598-018-30899-4
757 [Accessed January 22, 2021].
758 Cały A, Śliwińska MA, Ziółkowska M, Łukasiewicz K, Pagano R, Dzik JM, Kalita K, Bernaś T, Stewart
759 MG, Giese KP, Radwanska K (2021) PSD-95 in CA1 area regulates spatial choice depending
760 on age. J Neurosci Available at:
761 https://www.jneurosci.org/content/early/2021/01/14/JNEUROSCI.1996-20.2020 [Accessed
762 January 26, 2021].
763 Chen X, Nelson CD, Li X, Winters CA, Azzam R, Sousa AA, Leapman RD, Gainer H, Sheng M, Reese
764 TS (2011) PSD-95 Is Required to Sustain the Molecular Organization of the Postsynaptic

765 Density. J Neurosci 31:6329–6338 Available at:
766 http://www.jneurosci.org/cgi/doi/10.1523/JNEUROSCI.5968-10.2011 [Accessed November 4,
767 2020].
768 Cheng D, Hoogenraad CC, Rush J, Ramm E, Schlager MA, Duong DM, Xu P, Wijayawardana SR,
769 Hanfelt J, Nakagawa T, Sheng M, Peng J (2006) Relative and absolute quantification of
770 postsynaptic density proteome isolated from rat forebrain and cerebellum. Mol Cell Proteomics
771 MCP 5:1158–1170.
772 Chetkovich DM, Bunn RC, Kuo S-H, Kawasaki Y, Kohwi M, Bredt DS (2002) Postsynaptic targeting of
773 alternative postsynaptic density-95 isoforms by distinct mechanisms. J Neurosci Off J Soc
774 Neurosci 22:6415–6425.
775 de Oliveira Alvares L, Pasqualini Genro B, Diehl F, Molina VA, Quillfeldt JA (2008) Opposite action of
776 hippocampal CB1 receptors in memory reconsolidation and extinction. Neuroscience
777 154:1648–1655.
778 Ehrlich I, Klein M, Rumpel S, Malinow R (2007) PSD-95 is required for activity-driven synapse
779 stabilization. Proc Natl Acad Sci 104:4176–4181 Available at:
780 http://www.pnas.org/cgi/doi/10.1073/pnas.0609307104 [Accessed November 4, 2020].
781 Ehrlich I, Malinow R (2004) Postsynaptic Density 95 controls AMPA Receptor Incorporation during
782 Long-Term Potentiation and Experience-Driven Synaptic Plasticity. J Neurosci 24:916–927.
783 El-Boustani S, Ip JPK, Breton-Provencher V, Knott GW, Okuno H, Bito H, Sur M (2018) Locally
784 coordinated synaptic plasticity of visual cortex neurons in vivo. Science 360:1349–1354
785 Available at: https://www.sciencemag.org/lookup/doi/10.1126/science.aao0862 [Accessed
786 November 3, 2020].
787 Feng G, Mellor RH, Bernstein M, Keller-Peck C, Nguyen QT, Wallace M, Nerbonne JM, Lichtman JW,
788 Sanes JR (2000) Imaging Neuronal Subsets in Transgenic Mice Expressing Multiple Spectral
789 Variants of GFP. Neuron 28:41–51 Available at:
790 https://linkinghub.elsevier.com/retrieve/pii/S0896627300000842 [Accessed November 3,
791 2020].
792 Fischer A (2004) Distinct Roles of Hippocampal De Novo Protein Synthesis and Actin Rearrangement
793 in Extinction of Contextual Fear. J Neurosci 24:1962–1966 Available at:
794 http://www.jneurosci.org/cgi/doi/10.1523/JNEUROSCI.5112-03.2004 [Accessed November 4,
795 2020].
796 Fitzgerald PJ, Pinard CR, Camp MC, Feyder M, Sah A, Bergstrom HC, Graybeal C, Liu Y, Schlüter
797 OM, Grant SG, Singewald N, Xu W, Holmes A (2015) Durable fear memories require PSD-95.
798 Mol Psychiatry 20:901–912 Available at: http://www.nature.com/articles/mp2014161
799 [Accessed November 3, 2020].
800 Frankland PW, Bontempi B (2005) The organization of recent and remote memories. Nat Rev
801 Neurosci 6:119–130 Available at: http://www.nature.com/articles/nrn1607 [Accessed
802 November 4, 2020].
803 Gardoni F, Polli F, Cattabeni F, Di Luca M (2006) Calcium-calmodulin-dependent protein kinase II
804 phosphorylation modulates PSD-95 binding to NMDA receptors. Eur J Neurosci 24:2694–
805 2704 Available at: http://doi.wiley.com/10.1111/j.1460-9568.2006.05140.x [Accessed
806 November 4, 2020].
807 Garín-Aguilar ME, Díaz-Cintra S, Quirarte GL, Aguilar-Vázquez A, Medina AC, Prado-Alcalá RA
808 (2012) Extinction procedure induces pruning of dendritic spines in CA1 hippocampal field
809 depending on strength of training in rats. Front Behav Neurosci 6 Available at:
810 http://journal.frontiersin.org/article/10.3389/fnbeh.2012.00012/abstract [Accessed November
811 3, 2020].
812 Giese KP, Fedorov NB, Filipkowski RK, Silva AJ (1998) Autophosphorylation at Thr286 of the alpha
813 calcium-calmodulin kinase II in LTP and learning. Science 279:870–873.
814 Gipson CD, Kupchik YM, Shen H, Reissner KJ, Thomas CA, Kalivas PW (2013a) Relapse induced by
815 cues predicting cocaine depends on rapid, transient synaptic potentiation. Neuron 77:867–
816 872.
817 Gipson CD, Reissner KJ, Kupchik YM, Smith ACW, Stankeviciute N, Hensley-Simon ME, Kalivas PW
818 (2013b) Reinstatement of nicotine seeking is mediated by glutamatergic plasticity. Proc Natl
819 Acad Sci U S A 110:9124–9129.
820 Goh JJ, Manahan-Vaughan D (2013) Spatial Object Recognition Enables Endogenous LTD that
821 Curtails LTP in the Mouse Hippocampus. Cereb Cortex 23:1118–1125 Available at:
822 https://academic.oup.com/cercor/article-lookup/doi/10.1093/cercor/bhs089 [Accessed
823 November 4, 2020].
824 Gray JA (1982) The neuropsychology of anxiety: An enquiry into the functions of the septo-

825 hippocampal system. Behav Brain Sci 5:469–484 Available at:
826 https://www.cambridge.org/core/product/identifier/S0140525X00013066/type/journal_article
827 [Accessed November 3, 2020].
828 Grossberg S, Merrill JW (1992) A neural network model of adaptively timed reinforcement learning and
829 hippocampal dynamics. Brain Res Cogn Brain Res 1:3–38.
830 Hirsch SJ, Regmi NL, Birnbaum SG, Greene RW (2015) CA1-specific deletion of NMDA receptors
831 induces abnormal renewal of a learned fear response. Hippocampus 25:1374–1379.
832 Hoover WB, Vertes RP (2012) Collateral projections from nucleus reuniens of thalamus to
833 hippocampus and medial prefrontal cortex in the rat: a single and double retrograde
834 fluorescent labeling study. Brain Struct Funct 217:191–209 Available at:
835 http://link.springer.com/10.1007/s00429-011-0345-6 [Accessed November 4, 2020].
836 Huh KH, Guzman YF, Tronson NC, Guedea AL, Gao C, Radulovic J (2009) Hippocampal Erk
837 mechanisms linking prediction error to fear extinction: Roles of shock expectancy and
838 contextual aversive valence. Learn Mem 16:273–278 Available at:
839 http://learnmem.cshlp.org/cgi/doi/10.1101/lm.1240109 [Accessed November 4, 2020].
840 Ishizuka N, Weber J, Amaral DG (1990) Organization of intrahippocampal projections originating from
841 CA3 pyramidal cells in the rat. J Comp Neurol 295:580–623 Available at:
842 http://doi.wiley.com/10.1002/cne.902950407 [Accessed November 3, 2020].
843 Kaganovsky K, Plitt MH, Yang R, Sando R, Giocomo LM, Ding JB, Südhof TC (2022) Dissociating
844 encoding of memory and salience by manipulating long-term synaptic potentiation.
845 :2022.01.04.474865 Available at:
846 https://www.biorxiv.org/content/10.1101/2022.01.04.474865v1 [Accessed April 13, 2022].
847 Kajiwara R, Wouterlood FG, Sah A, Boekel AJ, Baks-te Bulte LTG, Witter MP (2008) Convergence of
848 entorhinal and CA3 inputs onto pyramidal neurons and interneurons in hippocampal area
849 CA1—An anatomical study in the rat. Hippocampus 18:266–280 Available at:
850 http://doi.wiley.com/10.1002/hipo.20385 [Accessed November 4, 2020].
851 Katz Y, Menon V, Nicholson DA, Geinisman Y, Kath WL, Spruston N (2009) Synapse Distribution
852 Suggests a Two-Stage Model of Dendritic Integration in CA1 Pyramidal Neurons. Neuron
853 63:171–177 Available at: https://linkinghub.elsevier.com/retrieve/pii/S0896627309005108
854 [Accessed November 3, 2020].
855 Kemp A, Manahan-Vaughan D (2007) Hippocampal long-term depression: master or minion in
856 declarative memory processes? Trends Neurosci 30:111–118 Available at:
857 https://linkinghub.elsevier.com/retrieve/pii/S0166223607000033 [Accessed December 21,
858 2020].
859 Kornau HC, Schenker LT, Kennedy MB, Seeburg PH (1995) Domain interaction between NMDA
860 receptor subunits and the postsynaptic density protein PSD-95. Science 269:1737–1740.
861 Kumaran D, Maguire EA (2006) An unexpected sequence of events: mismatch detection in the human
862 hippocampus. PLoS Biol 4:e424.
863 Lacagnina AF, Brockway ET, Crovetti CR, Shue F, McCarty MJ, Sattler KP, Lim SC, Santos SL,
864 Denny CA, Drew MR (2019) Distinct hippocampal engrams control extinction and relapse of
865 fear memory. Nat Neurosci 22:753–761 Available at: http://www.nature.com/articles/s41593-
866 019-0361-z [Accessed November 3, 2020].
867 Lattal KM, Abel T (2004) Behavioral impairments caused by injections of the protein synthesis inhibitor
868 anisomycin after contextual retrieval reverse with time. Proc Natl Acad Sci U S A 101:4667–
869 4672.
870 Lee S-H, Choi J-H, Lee N, Lee H-R, Kim J-I, Yu N-K, Choi S-L, Lee S-H, Kim H, Kaang B-K (2008)
871 Synaptic Protein Degradation Underlies Destabilization of Retrieved Fear Memory. Science
872 319:1253–1256 Available at:
873 https://www.sciencemag.org/lookup/doi/10.1126/science.1150541 [Accessed November 4,
874 2020].
875 Li J, Han Z, Cao B, Cai C-Y, Lin Y-H, Li F, Wu H-Y, Chang L, Luo C-X, Zhu D-Y (2017) Disrupting
876 nNOS-PSD-95 coupling in the hippocampal dentate gyrus promotes extinction memory
877 retrieval. Biochem Biophys Res Commun 493:862–868 Available at:
878 https://linkinghub.elsevier.com/retrieve/pii/S0006291X17317618 [Accessed November 3,
879 2020].
880 Mahmmoud RR, Sase S, Aher YD, Sase A, Gröger M, Mokhtar M, Höger H, Lubec G (2015) Spatial
881 and Working Memory Is Linked to Spine Density and Mushroom Spines Chapouthier G, ed.
882 PLOS ONE 10:e0139739 Available at: https://dx.plos.org/10.1371/journal.pone.0139739
883 [Accessed November 4, 2020].
884 Mamiya N, Fukushima H, Suzuki A, Matsuyama Z, Homma S, Frankland PW, Kida S (2009) Brain

Region-Specific Gene Expression Activation Required for Reconsolidation and Extinction of Contextual Fear Memory. J Neurosci 29:402–413 Available at: https://www.jneurosci.org/lookup/doi/10.1523/JNEUROSCI.4639-08.2009 [Accessed July 26, 2021].

Migaud M, Charlesworth P, Dempster M, Webster LC, Watabe AM, Makhinson M, He Y, Ramsay MF, Morris RGM, Morrison JH, O'Dell TJ, Grant SGN (1998) Enhanced long-term potentiation and impaired learning in mice with mutant postsynaptic density-95 protein. Nature 396:433–439 Available at: http://www.nature.com/articles/24790 [Accessed November 4, 2020].

Morris RGM, Moser EI, Riedel G, Martin SJ, Sandin J, Day M, O'Carroll C (2003) Elements of a neurobiological theory of the hippocampus: the role of activity-dependent synaptic plasticity in memory Bliss TVP, Collingridge GL, Morris RGM, eds. Philos Trans R Soc Lond B Biol Sci 358:773–786 Available at: https://royalsocietypublishing.org/doi/10.1098/rstb.2002.1264 [Accessed November 3, 2020].

Nader K, Schafe GE, Le Doux JE (2000) Fear memories require protein synthesis in the amygdala for reconsolidation after retrieval. Nature 406:722–726 Available at: http://www.nature.com/articles/35021052 [Accessed November 4, 2020].

Nagura H, Ishikawa Y, Kobayashi K, Takao K, Tanaka T, Nishikawa K, Tamura H, Shiosaka S, Suzuki H, Miyakawa T, Fujiyoshi Y, Doi T (2012) Impaired synaptic clustering of postsynaptic density proteins and altered signal transmission in hippocampal neurons, and disrupted learning behavior in PDZ1 and PDZ2 ligand binding-deficient PSD-95 knockin mice. Mol Brain 5:43 Available at: http://molecularbrain.biomedcentral.com/articles/10.1186/1756-6606-5-43 [Accessed November 4, 2020].

Neves G, Cooke SF, Bliss TVP (2008) Synaptic plasticity, memory and the hippocampus: a neural network approach to causality. Nat Rev Neurosci 9:65–75 Available at: http://www.nature.com/articles/nrn2303 [Accessed November 4, 2020].

Nikonenko I, Boda B, Steen S, Knott G, Welker E, Muller D (2008) PSD-95 promotes synaptogenesis and multiinnervated spine formation through nitric oxide signaling. J Cell Biol 183:1115–1127 Available at: https://rupress.org/jcb/article/183/6/1115/35388/PSD95-promotes-synaptogenesis-and-multiinnervated [Accessed November 3, 2020].

Noguchi J, Matsuzaki M, Ellis-Davies GCR, Kasai H (2005) Spine-Neck Geometry Determines NMDA Receptor-Dependent Ca2+ Signaling in Dendrites. Neuron 46:609–622 Available at: http://www.sciencedirect.com/science/article/pii/S0896627305002382 [Accessed January 15, 2021].

Nowacka A, Borczyk M, Salamian A, Wójtowicz T, Włodarczyk J, Radwanska K (2020) PSD-95 Serine 73 phosphorylation is not required for induction of NMDA-LTD. Sci Rep 10 Available at: https://www.ncbi.nlm.nih.gov/pmc/articles/PMC7005143/ [Accessed December 7, 2020].

Nusser Z, Lujan R, Laube G, Roberts JDB, Molnar E, Somogyi P (1998) Cell Type and Pathway Dependence of Synaptic AMPA Receptor Number and Variability in the Hippocampus. Neuron 21:545–559 Available at: http://www.sciencedirect.com/science/article/pii/S0896627300805656 [Accessed January 14, 2021].

Pamplona FA, Bitencourt RM, Takahashi RN (2008) Short- and long-term effects of cannabinoids on the extinction of contextual fear memory in rats. Neurobiol Learn Mem 90:290–293.

Ploghaus A, Tracey I, Clare S, Gati JS, Rawlins JN, Matthews PM (2000) Learning about pain: the neural substrate of the prediction error for aversive events. Proc Natl Acad Sci U S A 97:9281–9286.

Radulovic J, Tronson NC (2010) Molecular Specificity of Multiple Hippocampal Processes Governing Fear Extinction. Rev Neurosci 21:1–18 Available at: https://www.degruyter.com/view/j/revneuro.2010.21.1/revneuro.2010.21.1.1/revneuro.2010.21.1.1.xml [Accessed November 4, 2020].

Radwanska K, Medvedev NI, Pereira GS, Engmann O, Thiede N, Moraes MFD, Villers A, Irvine EE, Maunganidze NS, Pyza EM, Ris L, Szymańska M, Lipiński M, Kaczmarek L, Stewart MG, Giese KP (2011) Mechanism for long-term memory formation when synaptic strengthening is impaired. Proc Natl Acad Sci U S A 108:18471–18475 Available at: https://www.ncbi.nlm.nih.gov/pmc/articles/PMC3215030/ [Accessed November 6, 2020].

Ramanathan KR, Jin J, Giustino TF, Payne MR, Maren S (2018) Prefrontal projections to the thalamic nucleus reuniens mediate fear extinction. Nat Commun 9:4527 Available at: https://www.nature.com/articles/s41467-018-06970-z [Accessed July 29, 2021].

Restivo L, Vetere G, Bontempi B, Ammassari-Teule M (2009) The Formation of Recent and Remote Memory Is Associated with Time-Dependent Formation of Dendritic Spines in the

945 Hippocampus and Anterior Cingulate Cortex. J Neurosci 29:8206–8214 Available at:
946 https://www.jneurosci.org/content/29/25/8206 [Accessed July 29, 2021].
947 Royer S, Paré D (2003) Conservation of total synaptic weight through balanced synaptic depression
948 and potentiation. Nature 422:518–522 Available at:
949 http://www.nature.com/articles/nature01530 [Accessed November 3, 2020].
950 Schafe GE, Nader K, Blair HT, LeDoux JE (2001) Memory consolidation of Pavlovian fear
951 conditioning: a cellular and molecular perspective. Trends Neurosci 24:540–546 Available at:
952 https://linkinghub.elsevier.com/retrieve/pii/S016622360001969X [Accessed November 4,
953 2020].
954 Schnell E, Sizemore M, Karimzadegan S, Chen L, Bredt DS, Nicoll RA (2002) Direct interactions
955 between PSD-95 and stargazin control synaptic AMPA receptor number. Proc Natl Acad Sci U
956 S A 99:13902–13907.
957 Schuette PJ, Reis FMCV, Maesta-Pereira S, Chakerian M, Torossian A, Blair GJ, Wang W, Blair HT,
958 Fanselow MS, Kao JC, Adhikari A (2020) Long-Term Characterization of Hippocampal
959 Remapping during Contextual Fear Acquisition and Extinction. J Neurosci 40:8329–8342
960 Available at: http://www.jneurosci.org/lookup/doi/10.1523/JNEUROSCI.1022-20.2020
961 [Accessed November 3, 2020].
962 Stansley BJ, Fisher NM, Gogliotti RG, Lindsley CW, Conn PJ, Niswender CM (2018) Contextual Fear
963 Extinction Induces Hippocampal Metaplasticity Mediated by Metabotropic Glutamate Receptor
964 5. Cereb Cortex 28:4291–4304 Available at:
965 https://academic.oup.com/cercor/article/28/12/4291/4608047 [Accessed November 3, 2020].
966 Stein V, House DRC, Bredt DS, Nicoll RA (2003) Postsynaptic Density-95 Mimics and Occludes
967 Hippocampal Long-Term Potentiation and Enhances Long-Term Depression. J Neurosci
968 23:5503–5506 Available at: https://www.jneurosci.org/lookup/doi/10.1523/JNEUROSCI.23-13-
969 05503.2003 [Accessed May 4, 2021].
970 Steiner P, Higley MJ, Xu W, Czervionke BL, Malenka RC, Sabatini BL (2008) Destabilization of the
971 Postsynaptic Density by PSD-95 Serine 73 Phosphorylation Inhibits Spine Growth and
972 Synaptic Plasticity. Neuron 60:788–802 Available at:
973 https://linkinghub.elsevier.com/retrieve/pii/S0896627308008878 [Accessed November 4,
974 2020].
975 Sturgill JF, Steiner P, Czervionke BL, Sabatini BL (2009) Distinct Domains within PSD-95 Mediate
976 Synaptic Incorporation, Stabilization, and Activity-Dependent Trafficking. J Neurosci
977 29:12845–12854 Available at: http://www.jneurosci.org/cgi/doi/10.1523/JNEUROSCI.1841-
978 09.2009 [Accessed November 3, 2020].
979 Taft CE, Turrigiano GG (2014) PSD-95 promotes the stabilization of young synaptic contacts. Philos
980 Trans R Soc B Biol Sci 369:20130134 Available at:
981 https://royalsocietypublishing.org/doi/10.1098/rstb.2013.0134 [Accessed November 3, 2020].
982 Tronson NC, Schrick C, Guzman YF, Huh KH, Srivastava DP, Penzes P, Guedea AL, Gao C,
983 Radulovic J (2009) Segregated Populations of Hippocampal Principal CA1 Neurons Mediating
984 Conditioning and Extinction of Contextual Fear. J Neurosci 29:3387–3394 Available at:
985 http://www.jneurosci.org/cgi/doi/10.1523/JNEUROSCI.5619-08.2009 [Accessed November 4,
986 2020].
987 Troyner F, Bertoglio LJ (2021) Nucleus reuniens of the thalamus controls fear memory
988 reconsolidation. Neurobiol Learn Mem 177:107343 Available at:
989 https://www.sciencedirect.com/science/article/pii/S1074742720301878 [Accessed July 29,
990 2021].
991 Vallejo D, Codocedo JF, Inestrosa NC (2017) Posttranslational Modifications Regulate the
992 Postsynaptic Localization of PSD-95. Mol Neurobiol 54:1759–1776 Available at:
993 http://link.springer.com/10.1007/s12035-016-9745-1 [Accessed November 4, 2020].
994 Vertes RP, Linley SB, Hoover WB (2015) Limbic circuitry of the midline thalamus. Neurosci Biobehav
995 Rev 54:89–107 Available at: https://linkinghub.elsevier.com/retrieve/pii/S0149763415000160
996 [Accessed November 4, 2020].
997 Xu W, Sudhof TC (2013) A Neural Circuit for Memory Specificity and Generalization. Science
998 339:1290–1295 Available at:
999 https://www.sciencemag.org/lookup/doi/10.1126/science.1229534 [Accessed November 3,
1000 2020].
1001

SUPPLEMENTARY FIGURES

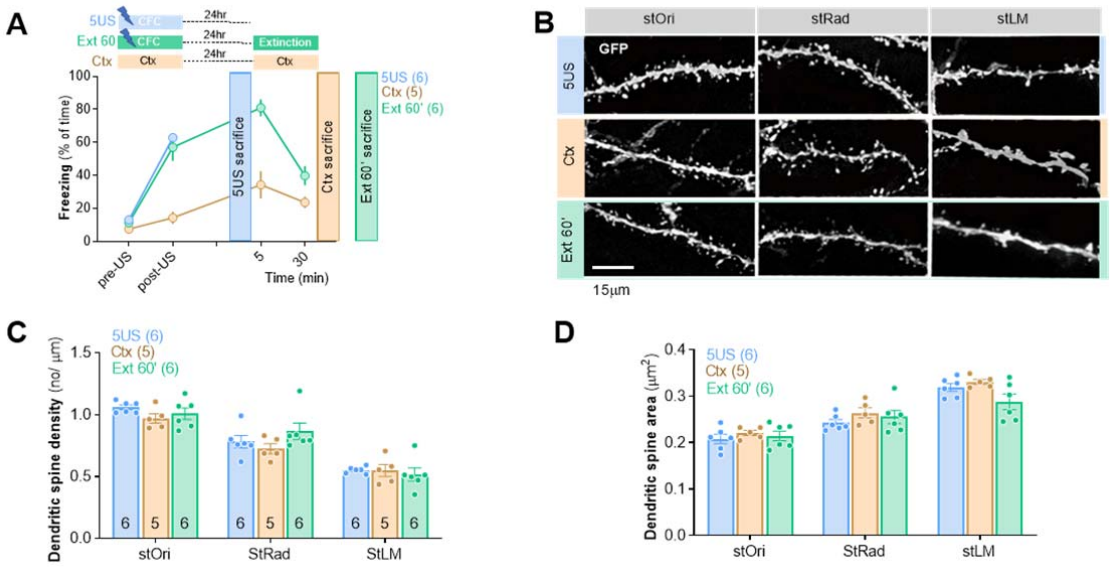

Supplementary Figure 1. **Synaptic plasticity induced by exposure to neutral context.** Dendritic spines were analysed in three domains of dendritic tree of dCA1 area in Thy1-GFP(M) male mice: stOri, stRad and stLM. **(A)** Experimental timeline and freezing levels of mice from three experimental groups: 5US (mice sacrificed 1 day after CFC; n = 6), Ctx (mice sacrificed immediately after the second exposure to novel context, no foot shocks were delivered, n = 5) and Ext 60' (mice sacrificed 60 minutes after contextual fear extinction session, n = 6). **(B)** Representative confocal images of dendrites (GFP) (maximum projections of z-stacks composed of 20 scans) are shown for three domains of the dendritic tree. **(C)** Summary of data showing dendritic spine density (repeated-measures ANOVA, effect of training: $F(2, 14) = 1.620$, $P = 0.233$). **(D)** Summary of data showing average dendritic spine area (repeated-measures ANOVA, effect of training: $F(2, 14) = 3.162$, $P = 0.074$). For C, D, each dot represents one mouse. For C means ± SEM are shown. For D, medians ± IQR are shown.

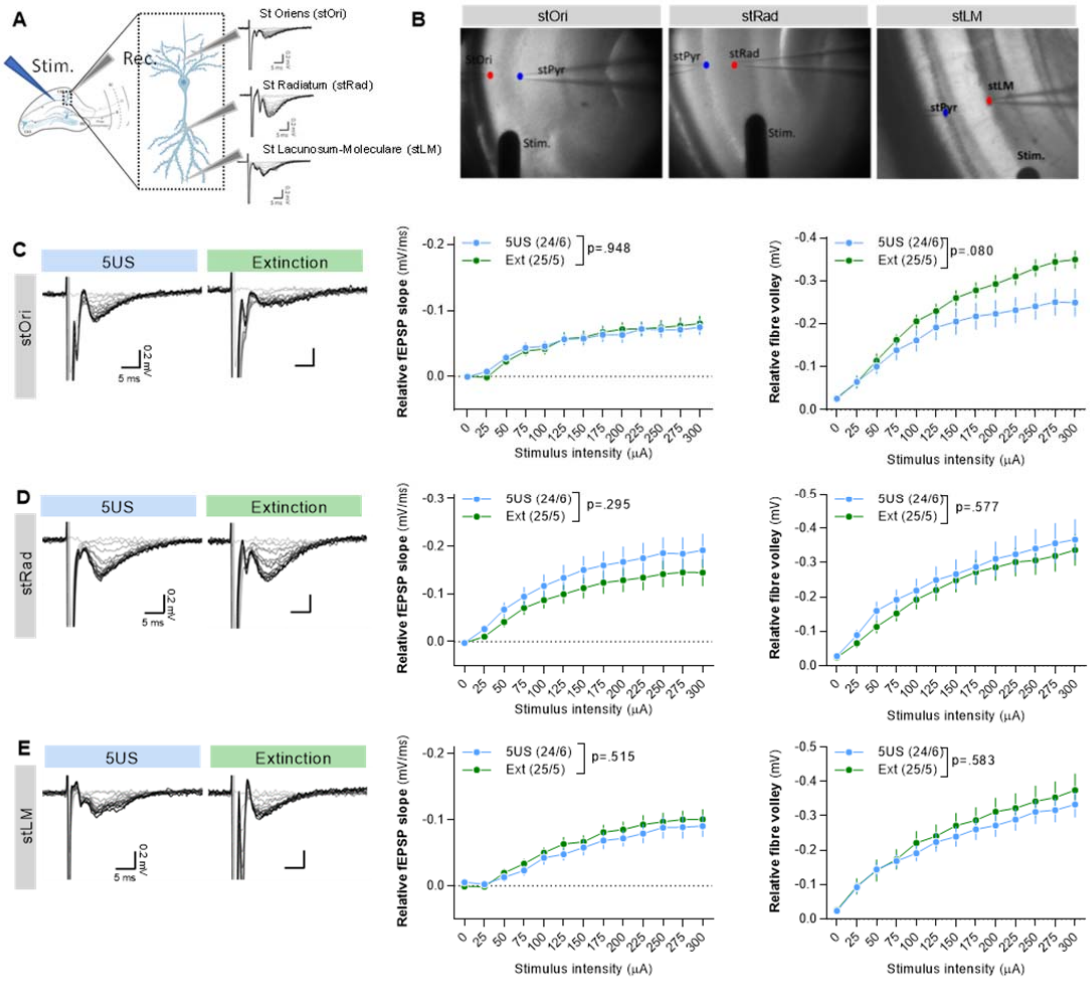

Supplementary Figure 2. Synaptic plasticity induced in dCA1 during contextual fear extinction training is compensatory. (A) Experimental design. **(B)** Microphotographs of recording setups. Stim-stimulation electrodes (Stim.) and two recording electrodes were placed in stPyr (blue dot) and stOri, stRad or stLM (red dots). **(C-E) (left)** Representative fEPSPs evoked by stimuli of different intensities, **(middle)** input–output functions for stimulus intensity (repeated-measures ANOVA, effect of virus: stOri, $F(1, 37) = 0.001$, $P = 0.971$; stRad: $F(1, 56) = 1.120$, $P = 0.294$; stLM: $F(1, 47) = 0.429$, $P = 0.515$) and **(left)** fibre volley recorded in response to increasing intensities of stimulation (repeated-measures ANOVA, effect of virus: stOri, $F(1, 43) = 3.198$, $P = 0.080$; stRad: $F(1, 47) = 0.314$, $P = 0.577$; stLM: $F(1, 44) = 0.305$, $P = 0.583$). The numbers of the analysed sections/mice per experimental group are indicated in the legends. Means ± SEM are shown on the graphs.

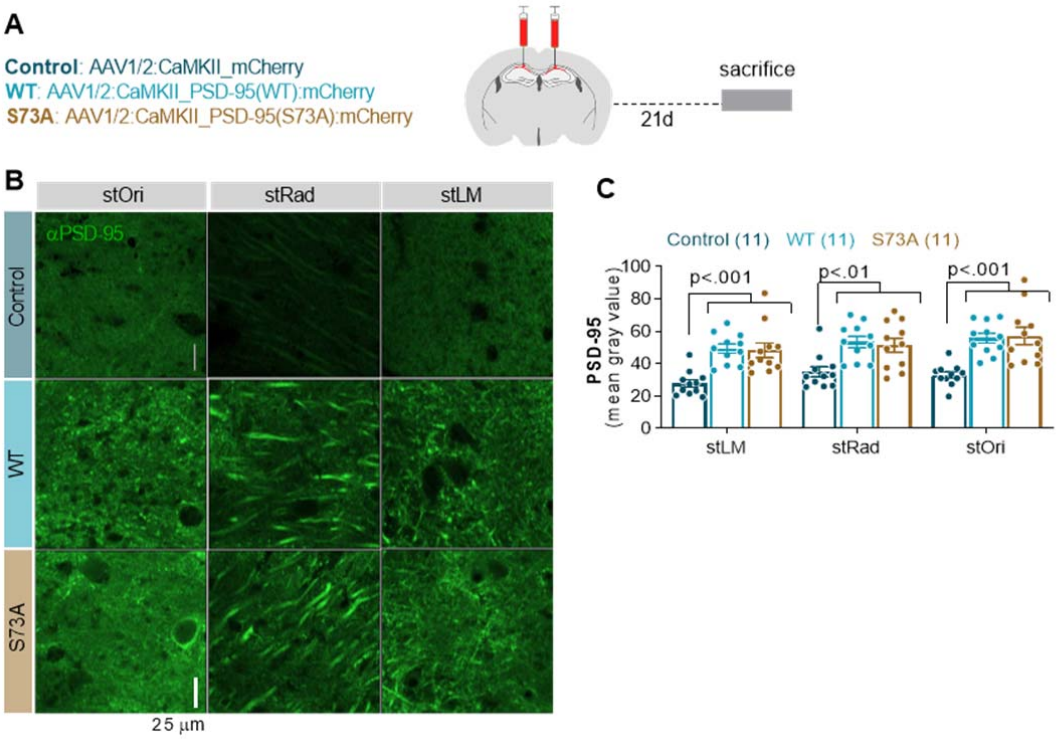

1031

1032 **Supplementary Figure 3. Validation of the viral vectors encoding PSD-95(WT) and PSD-**
1033 **95(S73A). (A)** Experimental timeline. C57BL/6J male mice were stereotactically injected in the dCA1
1034 with AAV1/2 encoding mCherry (Control, n=11) PSD-95(WT) (WT, n = 11) or PSD-95(S73A) (S73A, n
1035 = 11). Twenty one days later they were sacrificed. **(B)** Representative confocal scans of the PSD-95
1036 immunostaining in dCA1 strata and **(C)** summary of data showing PSD-95 levels (two-way ANOVA
1037 with Tukey's *post hoc* test, effect of virus: $F(2, 30) = 13.1$, $P < 0.001$).